

RECORD 2021/7

APPLYING GEOPHYSICS FOR 3D PALEOCHANNEL IMAGING IN THE GASCOYNE PROVINCE, WESTERN AUSTRALIA

by
S Jakica, L Brisbout and N de Souza Kovacs



Government of Western Australia
Department of Mines, Industry Regulation
and Safety

Geological Survey of
Western Australia





Government of **Western Australia**
Department of **Mines, Industry Regulation
and Safety**

RECORD 2021/7

APPLYING GEOPHYSICS FOR 3D PALEOCHANNEL IMAGING IN THE GASCOYNE PROVINCE, WESTERN AUSTRALIA

by
S Jakica, L Brisbout and N de Souza Kovacs

PERTH 2021



**Geological Survey of
Western Australia**

MINISTER FOR MINES AND PETROLEUM
Hon Bill Johnston MLA

DIRECTOR GENERAL, DEPARTMENT OF MINES, INDUSTRY REGULATION AND SAFETY
Richard Sellers

EXECUTIVE DIRECTOR, GEOLOGICAL SURVEY AND RESOURCE STRATEGY
Jeff Haworth

REFERENCE

The recommended reference for this publication is:

Jakica, S, Brisbout, L and de Souza Kovacs, N 2021, Applying geophysics for 3D paleochannel imaging in the Gascoyne Province, Western Australia: Geological Survey of Western Australia, Record 2021/7, 27p.

ISBN 978-1-74168-930-3

ISSN 2204-4345

Grid references in this publication refer to the Geocentric Datum of Australia 1994 (GDA94). Locations mentioned in the text are referenced using Map Grid Australia (MGA) coordinates, Zone 50. All locations are quoted to at least the nearest 100 m.

Disclaimer

This product uses information from various sources. The Department of Mines, Industry Regulation and Safety (DMIRS) and the State cannot guarantee the accuracy, currency or completeness of the information. Neither the department nor the State of Western Australia nor any employee or agent of the department shall be responsible or liable for any loss, damage or injury arising from the use of or reliance on any information, data or advice (including incomplete, out of date, incorrect, inaccurate or misleading information, data or advice) expressed or implied in, or coming from, this publication or incorporated into it by reference, by any person whosoever.

Published 2021 by the Geological Survey of Western Australia

This Record is published in digital format (PDF) and is available online at <www.dmirs.wa.gov.au/GSWApublications>.



© State of Western Australia (Department of Mines, Industry Regulation and Safety) 2021

With the exception of the Western Australian Coat of Arms and other logos, and where otherwise noted, these data are provided under a Creative Commons Attribution 4.0 International Licence. (<http://creativecommons.org/licenses/by/4.0/legalcode>)

Further details of geoscience products are available from:

Information Centre
Department of Mines, Industry Regulation and Safety
100 Plain Street
EAST PERTH WESTERN AUSTRALIA 6004
Telephone: +61 8 9222 3459 Email: publications@dmirs.wa.gov.au
www.dmirs.wa.gov.au/GSWApublications

Cover image: Wave and wind sculpted stromatolites at Flagpole Landing, Hamelin Pool in the world heritage site of Shark Bay, Western Australia (photo courtesy of Heidi Allen, DMIRS)

Contents

Abstract	1
Introduction	1
Study area and geological setting	2
Geomorphology of the Gascoyne Province	4
Methods	4
Passive seismic	4
The HVSr passive seismic method	4
Tromino instrument technical details	5
Survey design	6
Acquisition settings	6
AEM	7
2013 Capricorn AEM survey	7
2.5D AEM inversion	7
Bouguer gravity data	8
Results and data analysis	8
HVSr data quality	8
Velocity calibration at drillhole	12
Data visualization	12
HVSr vs elevation	12
3D depth to basement surface	20
Paleochannel geometry	20
Comparison of HVSr to other geophysical methods	20
2.5D AEM inversion	20
Gravity	22
Conclusions	22
References	26

Figures

1. Study area showing HVSr acquisition sites and AEM lines superimposed on total magnetic intensity data	2
2. Surface geology of the study area	3
3. Geological log from basement-intercepting drillhole SWMB007	4
4. Regional geomorphology showing drainage and major structural trends	5
5. Schematic HVSr spectral ratio data from a simple two-layer regolith-bedrock model	6
6. Tromino seismometers and three types of spike	6
7. HVSr spectral plot showing multiple frequency peaks detected by Tromino seismometer	7
8. High-resolution Bouguer gravity data showing the gravity low produced by the paleochannel	8
9. HVSr analysis in the proprietary Grilla software	9
10. H/V spectral ratio and amplitude spectra with 10% and 1% smoothing	10
11. Multi-peak HVSr recording	10
12. Shallow-basement HVSr recording showing a broad frequency peak	11
13. Two-maxima stratigraphic peak recording	12
14. Effects of noise removal	13
15. An example of an HVSr peak being determined based on the peak appearance at a neighbouring station	13
16. HVSr recording where north-south component is not responsive	14
17. Velocity (V_{s1}) estimation at drillhole SWMB007	14
18. Normalized HVSr values for all ten profiles plotted in 3D	15–19
19. A 3D representation of the basement surface	20
20. The 2.5D inversion profiles of the Capricorn 2013 AEM lines in the study area	21
21. AEM and aeromagnetic data mapping of the paleochannel profile	22
22. 3D view of the two 2.5D AEM lines in relation to the surface geology and ground gravity	23
23. Normalized HVSr data and AEM data, showing the base of the paleochannel interpreted from HVSr data	24
24. HVSr and gravity data shown as profiles	25

Tables

1. Shear-wave velocity for various materials	3
2. Tromino seismometer settings used in this study	7

Applying geophysics for 3D paleochannel imaging in the Gascoyne Province, Western Australia

by

S Jakica, L Brisboud and N de Souza Kovacs

Abstract

In predominantly arid Western Australia, paleochannels contain sand-dominated intervals that host water that is of potential interest to farmers, explorers and indigenous people. In many cases, the depth of the paleochannel marks the depth of cover above potentially prospective bedrock. The Cenozoic-era Yangibana paleochannel, composed dominantly of sands and clays, is incised into the Proterozoic granitic basement of the Gascoyne Province. Limited basement-intersecting drillholes are available from a groundwater study by Hastings Technology Metals Limited. These provide information on the depth of the paleochannel, which in this study is equivalent to the depth to basement. To better understand the geometry of the paleochannel and assess methods of estimating the depth to basement, we collected shallow-station passive seismic horizontal-to-vertical spectral ratio (HVSr) measurements and combined these with aeromagnetic, gravity and 2.5D inversion of airborne electromagnetic (AEM) data. An HVSr measurement at a Hastings Metals drillsite that intersects the basement provides information on the shear-wave velocity (V_s) of the regolith package overlying the basement. This V_s is applied to 256 HVSr sites, in ten profiles, to determine the depth and geometry of the paleochannel. The HVSr data indicate that the paleochannel changes orientation from northwesterly trending in the north of the study area to westerly trending in the south. Our study suggests that the paleochannel has a maximum depth of ~116 m (Traverse 1, site 14), where the channel changes orientation. In section, the geometry of the Yangibana paleochannel is similar to the geometry obtained from 2.5D inversion of two 2013 Capricorn TEMPEST regional AEM transects. The paleochannel is also observed in regional aeromagnetic data and high-resolution gravity traverses. In the Gascoyne Province study area, the HVSr passive seismic method is a cost-effective, easy and quick way to obtain the depth to basement.

KEYWORDS: AEM, depth to basement, HVSr, paleochannel, passive seismic

Introduction

Bilya is a network of cords going from one place to another, bringing life, giving water, feeding the land. In Noongar language and life, the word bilya begins at bily, meaning navel or belly button, becoming bilya the cord of life. Without rivers what would we have? As we rest beside it and ponder upon its continual nourishing we connect deeper to our existence and the true meaning of bilya. (Winmar and Bracknell, 2021)

Rivers and water sources have always played a major part in human life. From our ancestors' time more than 40 000 years ago until today, the search for water is one that has defined human existence. Being able to map the geometry of paleorivers, usually termed paleochannels, and also estimate their depths, is important for numerous reasons. In many terranes, the thickness of cover is defined by paleochannels and the depth to economically important basement geology is a crucial search that defines resource prospectivity. More fundamentally, water sources are required for human habitation or agricultural needs. Paleochannels are a potential source of groundwater to meet these needs. In addition, paleochannels can also host mineral deposits such as potash and uranium (Owers et al., 2016). In isolated semi-desert environments like

the Gascoyne Province, understanding the geometry of paleochannels provides crucial information on potential groundwater resources, which can be the main sustainable water source in the region.

As paleochannels are buried ancient rivers, their discovery and definition are made mostly through geophysical techniques. The airborne electromagnetic (AEM) method has been used extensively in the past to explore under thick sedimentary cover (Mackey et al., 2000; Paterson et al., 2017; Munday et al., 2018; Roach, 2018), including paleochannel mapping (Jiang et al., 2019; Krapf et al., 2019). Increasingly, shallow passive seismic methods are also being used for determining the thickness of the cover (lbs-von Seht and Wohlenberg, 1999; Smith et al., 2013; Scheib, 2014; Jakica, 2018; Kumar et al., 2018). Of relevance to this study, Owers et al. (2016) demonstrated that the horizontal-to-vertical spectral ratio (HVSr) passive seismic method with data acquired by Tromino instruments was successful in mapping paleovalley geometry to assist in potash exploration.

Drilling by Hastings Technology Metals Limited indicated the presence of an aquifer within the Yangibana paleochannel in the Gascoyne Province, Western Australia. Due to the limited drilling in the area, the geometry and depth of the channel were unknown. To understand the geometry of the Yangibana paleochannel and hence the likely extent of the

aquifer, the Geological Survey of Western Australia (GSWA) carried out shallow passive seismic data acquisition in August 2018 (Fig. 1). The acquisition was designed on the basis of regional aeromagnetic and AEM data, and high-resolution gravity data, and was carried out using the Tromino HVSR passive seismic technique (see the following for details of the method: Micromed, 2012; MoHo, 2017; Meyers, 2017; Owers et al., 2016). By using complementary geophysical methods, these data can shed light on the best approaches to map paleochannels at different scales. In particular, this study aimed to test the use of HVSR data to map the geometry of the paleochannel at the target scale and to compare the results with AEM data. Further, the study investigates the best technique for mapping paleochannels from regional to the target scale.

The study demonstrates how different geophysical techniques can improve the currently available paleochannel maps of Western Australia (see Bell et al., 2012). The methods used in this study add depth information to the paleochannel geometry and increase its resolution.

Study area and geological setting

The study area is located in the Paleoproterozoic Gascoyne Province of the Capricorn Orogen (Fig. 1). Outcropping basement is present only in the east of the study area and is dominated by granitic rocks of the Paleoproterozoic

Durlacher Supersuite. Minor sandstone, siltstone and dolostone of the Paleoproterozoic Yilgatherra Formation, of the Edmund Basin, are also present (Fig. 2) (Martin et al., 2004). The bedrock is intruded by sills, dykes and veins of ferrocarnatite and rare-earth-element-bearing (REE-bearing) ironstone of the 1300–1280 Ma Gifford Creek Ferrocarnatite Suite (Border et al., 2017). Border et al (2017) defines ironstones as hydrothermal veins comprised of iron oxides and residual carbonate minerals. The ironstone outcrops throughout the Yangibana area are interpreted as weathered and leached remnants of phosphorite intrusions (Border et al., 2017). The ironstone dykes are surrounded by relatively narrow haloes of fenitic alteration and are locally associated with quartz veins (Hastings Technology Metals Limited, 2017).

In the central and west of the study area, the units of the Gascoyne Province are covered by Cenozoic alluvial units deposited by the Edmund River system (Fig. 2) (Martin et al., 2004). Most of the surface of the study area, including along the passive seismic traverses, is covered by an alluvial unit of sand and gravel with ferruginous cement.

Based on the auger drilling in the study area, regolith stratigraphy comprises colluvium units overlying clay, silts, occasional calcrete, sands and gravel before reaching saprolite and the granitic basement (Fig. 3) (Jefferson and McDougall, 2019).

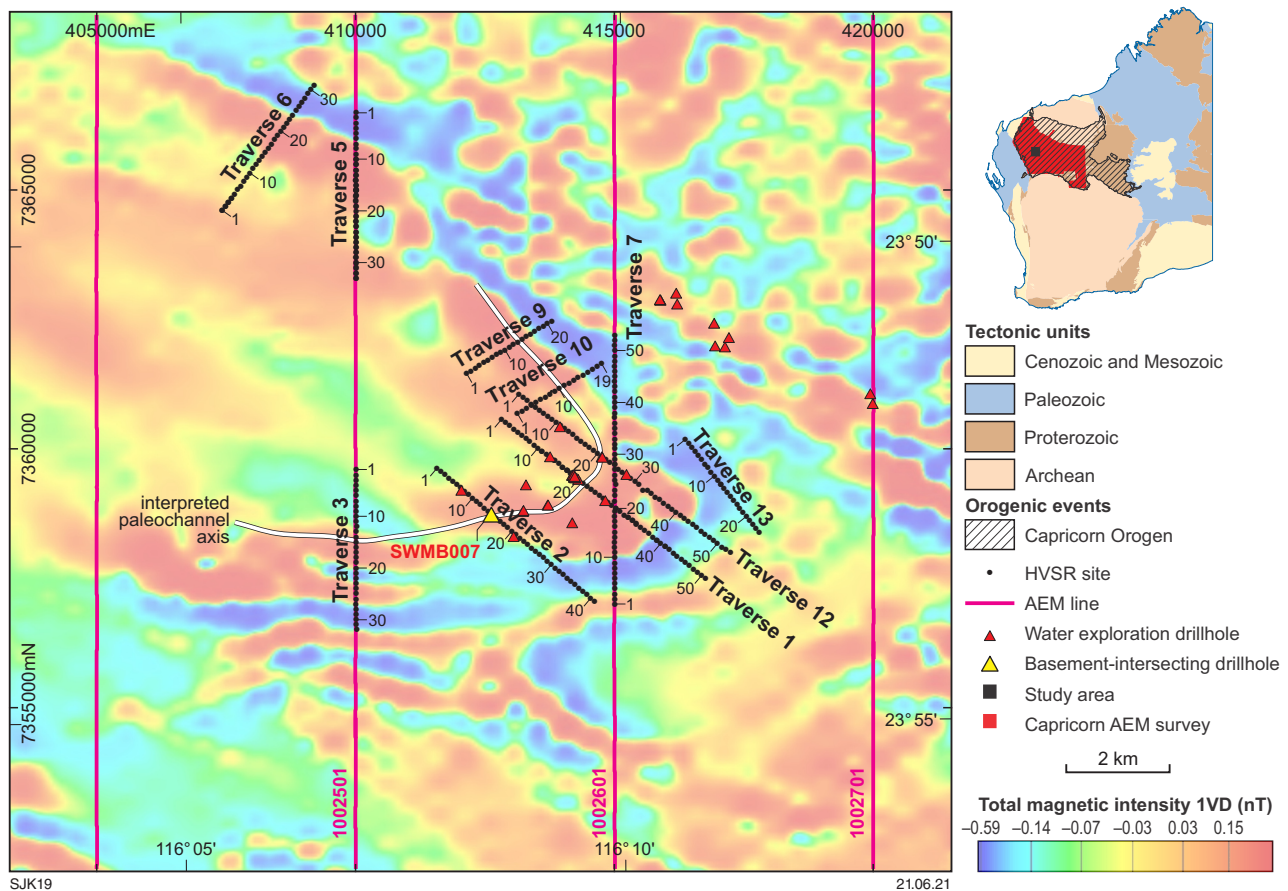


Figure 1. Study area showing passive seismic traverses, the two Capricorn 2013 AEM survey lines used in this study, interpreted paleochannel axis and the locations of water exploration drillholes (Geological Survey of Western Australia, 2020). The background image is the first vertical derivative of the total magnetic intensity data

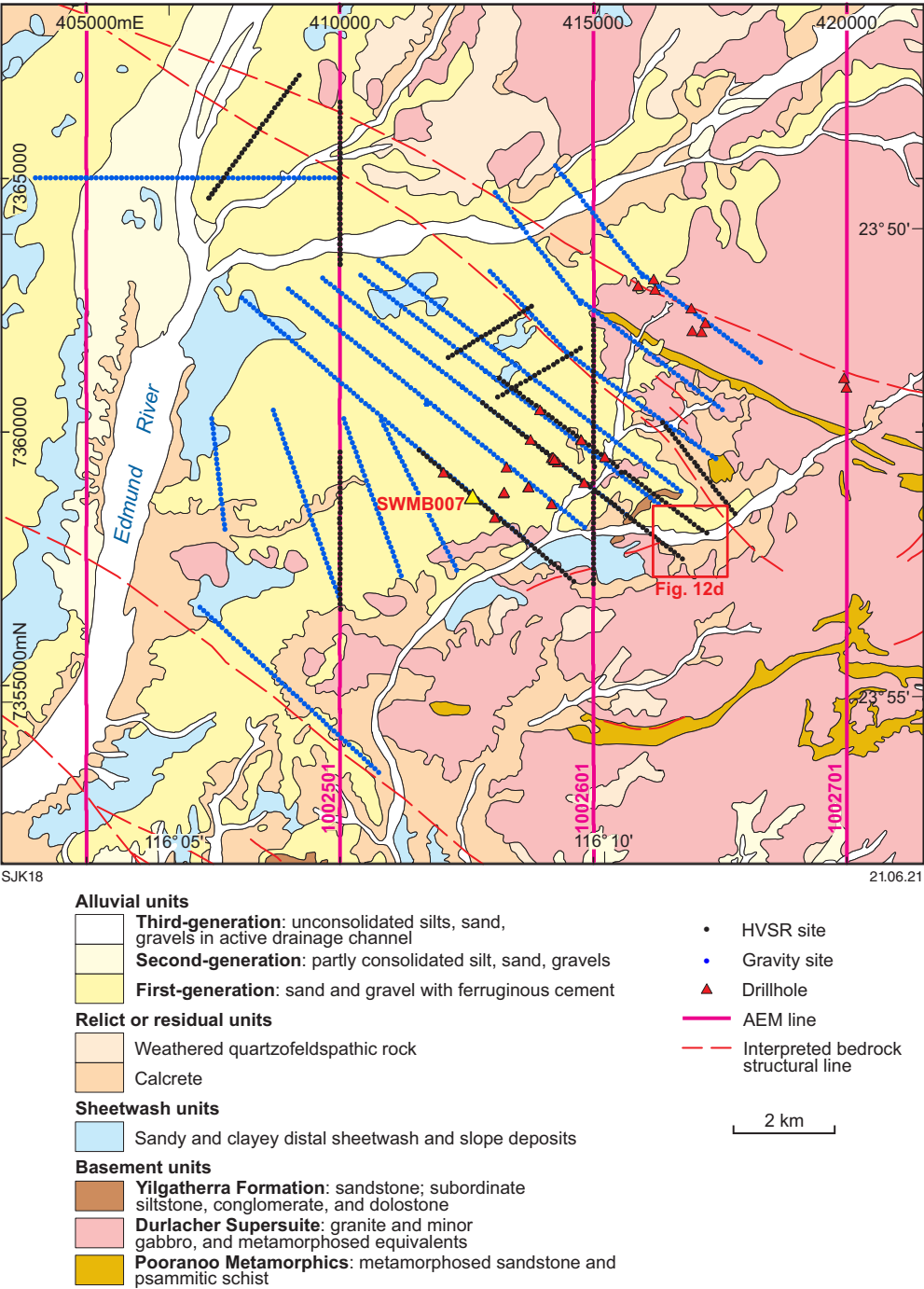


Figure 2. Surface geology of the study area (modified from Martin et al., 2004), showing passive seismic traverses, gravity stations, AEM survey lines and water exploration drillholes

Table 1. Shear-wave velocity for various materials

Lithology	Vs (m/s)	Source
clay, tufs	180	
clay and sandy silt	200	
sand and gravel	300	Micromed, 2009; Ibs-von Seht and Wohlenberg, 1999
gravel and altered/soft rock	400	
soft/layered sedimentary rock	500	
alluvium (at 30 m depth)	257-338	Collins et al., 2006
Archean granite (in WA, at 30 m depth)	474-1232	
rock	>750	Scheib, 2014
hard rock	>1500	Scheib, 2014; Ibs-von Seht and Wohlenberg, 1999

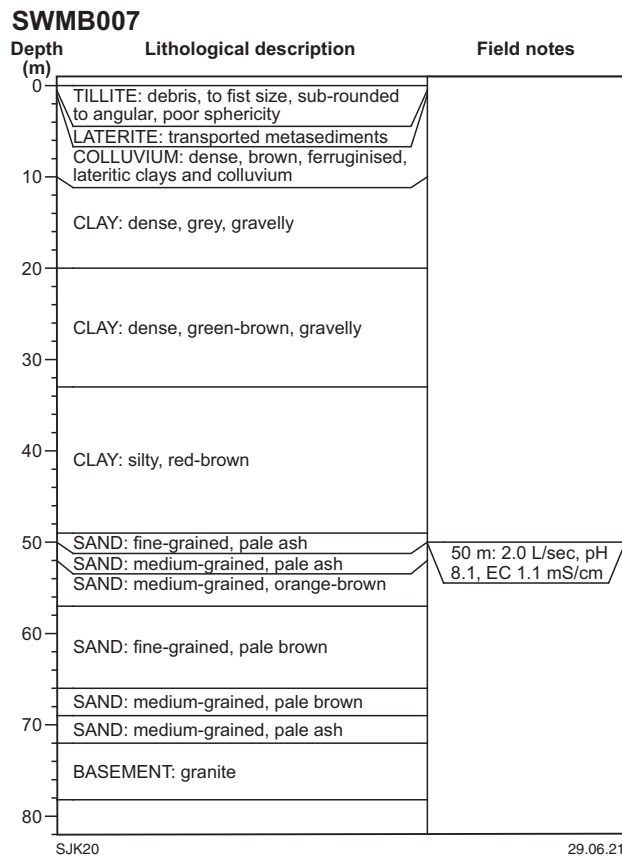


Figure 3. Geological log from basement-intersecting drillhole SWMB007, illustrating the paleochannel stratigraphy (information provided by Hastings Technology Metals)

Geomorphology of the Gascoyne Province

The regional geomorphology of the study area consists of undulating hills striking west-northwesterly, parallel to the major faults (Fig. 4a). Valleys are up to 2.5 km wide (Edmund River), with flat-bottomed, braided river channels filled with alluvial and sheetwash deposits that are rich in quartz and lithic clasts derived from nearby hills, as well as localized calcrete (Fig. 4b,c). The drainage morphology defines a dendritic to rectangular drainage network (Fig. 4a). Rivers and creeks are mostly dry with seasonal, occasional water flow during and after main rain episodes (Petheram et al., 2008).

Methods

Passive seismic

The HVSR passive seismic method

The short-station (i.e. short recording time) passive seismic method used in this study is the HVSR method (or Nakamura technique) that uses three-component measurements (comprising relative north–south or X, relative east–west or Y and up–down or Z components) of ambient noise (or microtremor) as a seismic source to determine and evaluate fundamental seismic resonance frequency (Nakamura, 1989; Lane et al., 2008).

Originally developed to help define the seismic hazard in Japan (Nakamura, 1989), the HVSR method is now broadly used across different industries such as resource exploration, the hydrogeological, geotechnical and environmental sectors and construction. In mineral and water exploration, the HVSR method is used to determine the depth to basement or other stratigraphic boundaries. The base of a paleochannel incised into basement is an excellent candidate for HVSR (Scheib, 2014; Owers et al., 2016). HVSR is a rapid and non-invasive method that measures ambient, natural noise in the subsurface at the broad range of frequencies from 0.1 to 2048 Hz, over a set time interval (generally between five and sixty minutes). Signals above 1 Hz are usually mapping shallow basement and/or intra-regolith interfaces. These signals are produced by microtremors, i.e. near-surface ambient vibrations from anthropic sources such as traffic, agriculture or industrial noise (Chandler and Lively, 2014; Meyers, 2017). Signals below 1 Hz are microseisms and are produced by natural forces, such as ocean waves, wind and deeper micro-seismic events (Chandler and Lively, 2014; Meyers, 2017). These signals are usually mapping deeper regolith-to-basement interfaces (Meyers, 2017).

The HVSR method is based on a simple two-layer system such as regolith overlying bedrock. The resonance frequency is amplified with a stronger and sharper impedance contrast boundary between the two units (Fig. 5). A very strong impedance contrast is generally observed at the regolith–bedrock boundary due to vastly different properties of the crystalline basement and less consolidated regolith material. The impedance contrast results from the different shear-wave velocities (V_{s1} , V_{s2}) of the two layers and their respective densities (Fig. 5). The shear-wave velocity is a measure of how fast the ambient noise travels through a rock unit. Some examples of shear-wave velocities for different materials, ranging from soft soils to hard rock, are listed in Table 1. The greater the difference in shear-wave velocity between the two units, the larger the impedance contrast, and the greater the resonance frequency peak in HVSR. The resonance frequency (f_z) at which the impedance contrast is measured is a function of the depth of the boundary between the two units (Fig. 5):

$$f_z = (V_s/4h) \quad (\text{Equation 1})$$

This relationship between the frequency (f_z), shear-wave velocity of the unit in question (V_{s1} ; Fig. 5) and the thickness of the unit (h_1 ; Fig. 5) is the basis of the short-station passive seismic approach to estimating cover thickness. In this study, the resonance frequency peak produced by an impedance contrast at depth is also referred to as a stratigraphic peak. Frequency peaks produced by noise, for example wind, are referred to as non-stratigraphic peaks.

There are some limitations to using the HVSR technique that must be considered when interpreting results or designing surveys. If the overlying and underlying units have similar petrophysical properties, or there is a gradational contact between units, the resulting weakened impedance contrast means that the resonance frequency and hence the HVSR peak are poorly defined (SESAME European Research Project, 2004; Lane et al., 2008). While mapping the thickness of till units in north America, Lane et al. (2008) found that a low impedance contrast between the till and deeply weathered bedrock resulted in a poorly defined HVSR peak. In areas characterized by deep weathering, a poorly

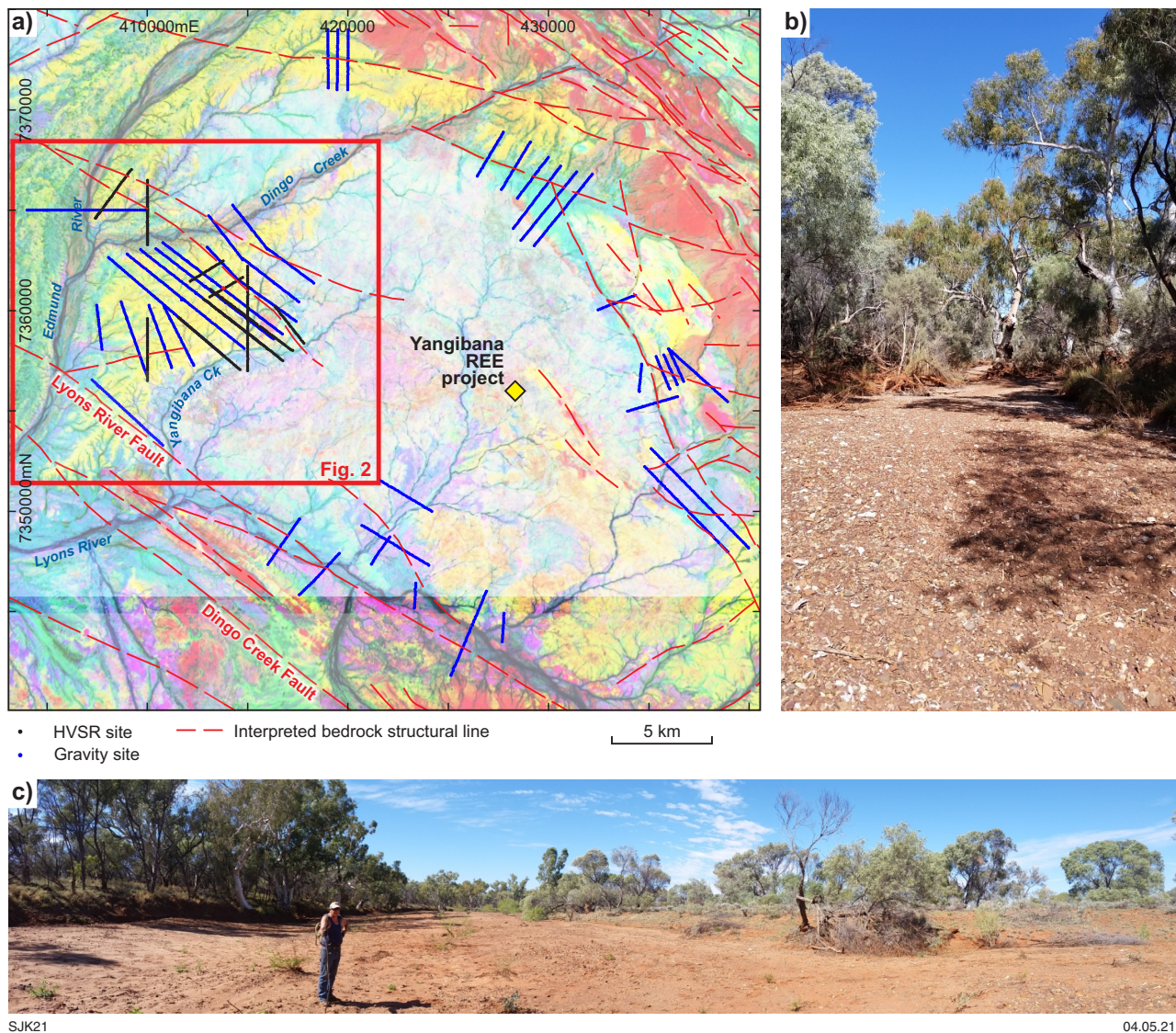


Figure 4. Regional geomorphology with the study area outlined in red: a) the broader scale of the area showing the drainage morphology and major structural trends (background image is the Landsat AGSO ratio); b) unnamed creek, Yangibana upper tributary, photo showing alluvial deposits in the dry channel consisting of quartz vein clasts, lithic fragments, coarse quartz and lithic sand and minor calcrete; c) the dry bed of Dingo Creek braided river channel, with vegetated sand bar to the right

defined HVSR peak might be produced by a gradational increase in velocity and reduced impedance contrast at the regolith–basement interface. In such environments, it is recommended to obtain a good coupling of the instrument with the ground by digging a shallow hole and placing the instrument in the hole. This will reduce the chance of the noise further masking the HVSR reading (Feldpausch, 2017). Further, low-amplitude velocity responses can be amplified by normalization during data processing (see *Data visualization* section for further details).

Tromino instrument technical details

The Tromino is a three-component seismometer that measures ambient seismic noise in the subsurface in the range of frequency of 0.1 to 200 Hz (MoHo, 2017). Each instrument has three channels connected to three orthogonal electrodynamic velocimeters with selectable gain for seismic tremor acquisition (MoHo, 2017). The acquired data are stored in an internal memory card and transferred to a PC using Grilla v. 8 proprietary software

provided by MoHo Science and Technology. The system can also acquire in continuous mode and send data to a PC through the Tromino Manager software tool (MoHo, 2017). This study's Tromino settings and device set-up in the field, detailed in Table 2, were chosen in accordance with supplied recommendations and previous studies done by various researchers. The following were the sources for these set-up decisions: Micromed, 2009, 2012; Chandler and Lively, 2014; Scheib, 2014; Owers et al., 2016; Meyers, 2017; MoHo, 2017.

The Tromino instrument can detect multiple frequency peaks where there are strong impedance contrasts between layers. Peaks will occur at the resonant frequency corresponding to each layer, with deeper impedance contrasts producing lower frequency peaks (Fig. 7).

The GSWA maintains five short-station seismic HVSR Tromino seismometers: one Tromino 3G Zero (purchased in 2012) and four Tromino 3G ENGy units (purchased in 2017) (Fig. 6a,b). These Tromino units are compact (10 x 14 x 8 cm), lightweight (1.1 kg), have low energy consumption and are easy to use for capturing high-resolution seismic noise measurements (MoHo, 2017).

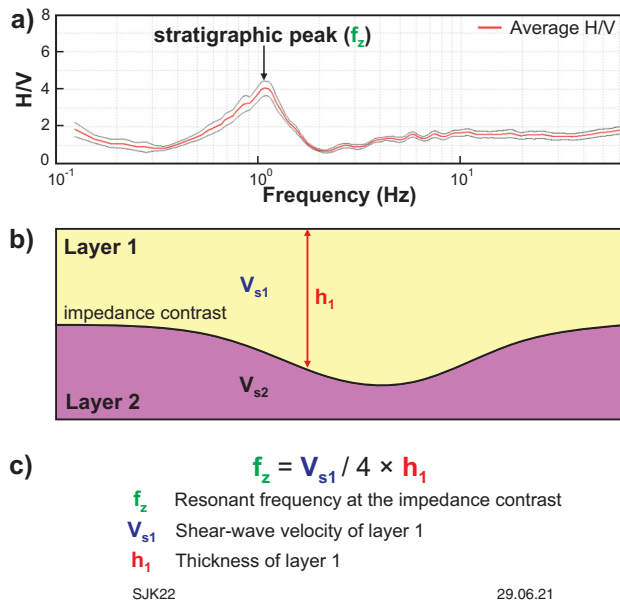


Figure 5. Schematic HVSR spectral ratio data from a simple two-layer regolith-bedrock model: a) H/V spectral ratio plot with a peak at the resonance frequency (f_z) indicating an impedance contrast at depth; b) simple two-layer regolith-bedrock model with an impedance contrast at depth (h_1); c) Equation 1 showing the relationship between the resonance frequency, shear-wave velocity (V_{s1}) and depth to the impedance contrast (h_1)

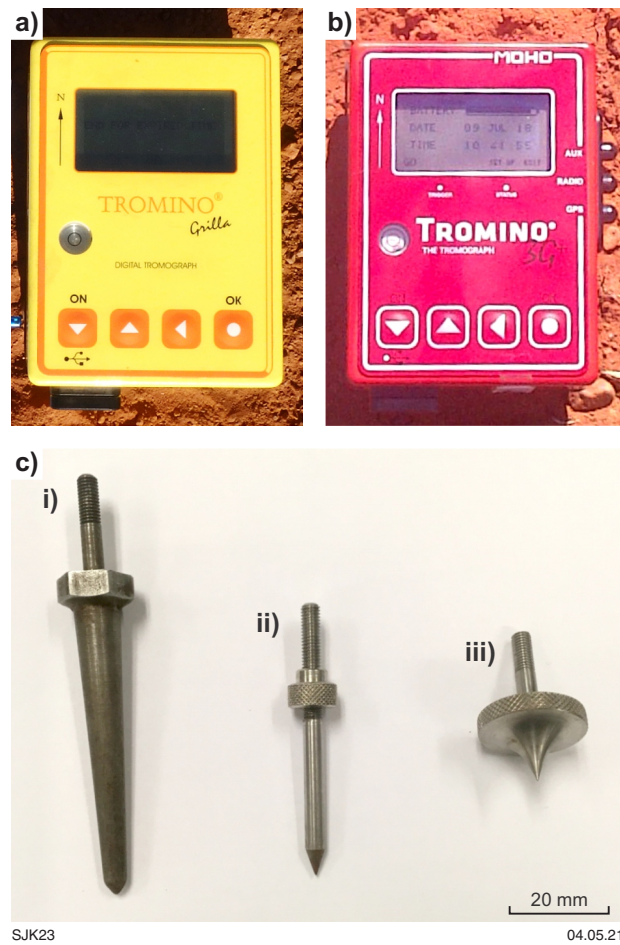


Figure 6. Tromino seismometers: a) Tromino 3G ZERO; b) Tromino 3G ENG Y; c) spikes for ground coupling (i) custom-made, 10 cm total length and 6-cm penetration length; ii) long spike, 6 cm total length and 4-cm penetration length; iii) short spike, 3 cm total length)

Tromino HVSR data are compatible with data acquired using more expensive and less portable seismometer systems, such as Guralp (Castellaro and Mulargia, 2009; Chandler and Lively, 2014). The Tromino 3G ZERO model requires two AA batteries, while the Tromino 3G ENG Y is equipped with internal lithium-ion rechargeable batteries, allowing for ~100 hours of continuous measurements (MoHo, 2017). Other updates from the Tromino 3G ZERO to Tromino 3G ENG Y model are a built-in GPS module with internal or external antenna and a built-in radio module for the synchronization of several Tromino ENG Y instruments (MoHo Science and Technology, 2017). Synchronization of the Tromino units can be used for modal studies of structures or for small to mid-scale seismic arrays. In addition to the HVSR passive seismic technique, radio synchronization and radio trigger enables Tromino ENG Y units compatible with ReMi (refraction microtremor), ESAC (extended spatial auto-correlation), SPAC (spatial auto-correlation), MASW (multi-channel analysis of surface waves), and P- and S-wave refraction techniques (MoHo Science and Technology, 2017).

Survey design

In August 2018, the GSWA acquired shallow, short-station passive seismic data over the Yangibana paleochannel. The acquisition was carried out using the single-station HVSR method with Tromino instruments (Fig. 6). Data were acquired over 10 traverses that varied in length between 2 and 5.2 km. Three traverses followed high-resolution gravity profiles, three followed AEM lines from the 2013 Capricorn regional survey (CGG, 2013) and eight crossed the interpreted magnetic channel fill (Figs 1, 2). The survey was designed so that HVSR data could be compared with AEM and Bouguer gravity data, and also to test whether the magnetic anomaly is caused by magnetic channel fill.

Acquisition settings

The terrain was mostly clear of vegetation, with sandy to pisolithic ground. To ensure good coupling with the ground and optimal signal transfer, three spikes were mounted into each Tromino instrument, which was then pushed into the ground (Fig. 6). This study used three different types of spike (Fig. 6c), dependent on the ground conditions, to ensure good ground coupling: 6 cm-long spikes with 4-cm penetration length; short, round spikes (3 cm total length) and custom-made conical-shaped spikes 10 cm long with 6-cm penetration length. The long and short spikes come as standard equipment with the instruments from the manufacturer. The custom-made spikes (suitable for Tromino ENG Y units only) were made by the Centre for Exploration Geophysics, WA School of Mines, Curtin University, for better coupling. Their conical design is more resemblant of spikes used for conventional reflection seismic geophones.

Each instrument was oriented to magnetic north and the levelling bubble used to ensure the device was horizontal. At the time of the survey, the declination of the magnetic grid to true north was insignificant (0.024 degrees) and hence no correction to true north was necessary (determined by reference to the [Geoscience Australia website](#)). At the pisolith-rich sites, it was difficult to obtain full penetration depths for the spikes while simultaneously keeping the instrument level.

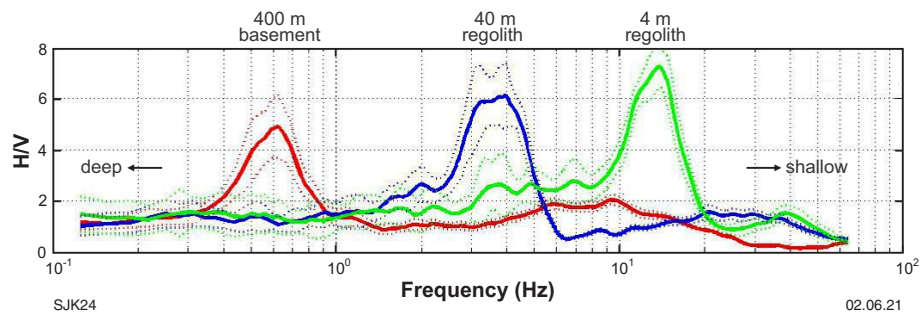


Figure 7. HVSR spectral plot showing multiple frequency peaks detected by Tromino seismometer (modified from MoHo, 2017). In this example, the deeper basement interface is represented by a lower frequency peak and the shallower intra-regolith interfaces by higher frequency peaks

Table 2. Tromino seismometer settings used in this study

<i>Tromino Settings</i>	<i>Select</i>
On	
Set up	ok
Initial Menu	ok
Acquisition	Program 1
Acquisition mode	high gain channel
Acquisition sampling	128 Hz
Acquisition length	20 minutes
Aquire	ok
Initial menu	switch off

Tight coupling is much more important than a levelled instrument; hence the preference was to insert spikes completely into the ground rather than achieve perfect levelling of the instrument. If vegetation, loose rocky soils and pisoliths were present, the acquisition area was cleared or deepened. Occasionally a drill was used to initiate drillholes for the long MoHo and custom-made spikes. The drill bits used were always thinner than the spikes to avoid loosening the hole and therefore affecting mechanical coupling. The drilled holes were also shorter than the spikes' penetration lengths, and were only used in the areas where large pisoliths prevented the spikes from penetrating the ground. The short MoHo spikes were used only when the ground was too stiff for significant spike penetration (representing less than 10 per cent of monitoring stations). HVSR readings were taken over a 20-minute recording period, and these measurements were made every 100 m along each of the ten traverses. Acquired data were downloaded at the end of each day and rapid in-field quality control was performed. If the data were too noisy due to poor coupling or wind, the measurements were repeated.

AEM

2013 Capricorn AEM survey

The Yangibana paleochannel is located within the limits of the regional 2013 Capricorn TEMPEST AEM survey (Fig. 1). The survey was conducted as part of the Western Australia Exploration Incentive Scheme (EIS) and managed by Geoscience Australia on behalf of the GSWA. The total coverage of the survey was 30 119 line kilometers flown

within 60 flights (CGG, 2013). The line spacing for this survey was 5000 metres. In the study area, the line orientation is north–south.

2.5D AEM inversion

AEM data were inverted to provide depth profiles of electrical conductivity. Electrical conductivity variations are commonly caused by conductive materials such as clay, graphite, salt or saline water and sulfide-bearing minerals. Horizontal resolution of the AEM inverted sections depends on the distance between the flight lines and the frequency of measurements along the flight lines, while vertical resolution varies from metres to tens of metres depending on local electrical conductivity of the ground.

The GSWA employed Intrepid Geophysics to perform 2.5D (2D geology, 3D source) inversions on two small areas (Fortnum and Edmund Station) from the Capricorn 2013 TEMPEST AEM survey (Paterson, 2019). Portions of two AEM lines (1002501 and 1002601) traverse the Yangibana paleochannel study area (Fig. 1). The data were inverted using proprietary Intrepid Geophysics 2.5D inversion code. The code is an updated version of ArjunAir code, a product of CSIRO/AMIRA project P223F (Wilson et al., 2006). The 2.5D inversion is based on a full-wave solution to Maxwell's equation using a frequency-domain and spatial-Fourier-domain finite element method (Silic et al., 2015; Silic et al., 2018). The advantage of the 2.5D inversion code over other more conventional methods, such as conductivity–depth images (CDI) and 1D inversion, is that the 2.5D code can use all the measured components in a joint inversion and can forward-model using a full 3D source (Paterson et al., 2017). This produces a better constrained prediction of geological structures and features that are poorly represented by 1D assumptions (Paterson et al., 2017). Paterson et al (2017) demonstrated the improvement gained using the 2.5D AEM inversion method when mapping water aquifers and paleochannels, resulting in cleaner imaging of the channel geometry compared to CDI sections and results of 1D inversions.

The detailed report on the 2.5D inversion methodology over the study area (Paterson, 2019), AEM data and GeoModeller project can be downloaded from the GSWA data portal [GeoVIEW.WA](#) (MAGIX Surveyblocks Polygons – MAGIX Registration Number 70825).

Bouguer gravity data

High-resolution gravity data were acquired by Hastings Technology Metals to assist with groundwater exploration. Gravity data were collected in two campaigns – the first a reconnaissance-scale survey, targeting creeks surrounding a dome of Pimbyana Granite (Jefferson and McDougall, 2019) of the Paleoproterozoic Durlacher Supersuite. The second survey focused on the Yangibana paleochannel (Fig. 2). In the Yangibana project area, gravity data were collected along 17 traverses with stations spaced 100 m apart (Fig. 8). Gravity data from both surveys have been reduced and corrected by Newexco Exploration Pty Ltd (Amann, 2018). A Bouguer spherical cap correction was applied assuming a density of 2.67 g/cm³ and a first-order polynomial, which estimates the regional field from more distance and deeper sources, was subtracted from the data (Amann, 2018). Removing a regional field enhances the higher frequency components of the gravity data, including the gravity response produced by a paleochannel. A paleochannel or an increase in the depth of basement would be expected to produce a corresponding decrease in Bouguer gravity data.

Bouguer gravity data from Hastings were imported into Geosoft Oasis montaj v. 9.9.1 and gridded using minimum curvature to a cell size of 100 m. The resulting Bouguer gravity image shows a gravity low in the east, extending in two narrow arms to the northwest and west (Fig. 8). The gravity data indicates a paleochannel that changes direction from northwesterly to westerly and is deepest in the east where the paleochannel changes orientation. The suggested trend of the paleochannel, interpreted largely from Bouguer gravity data, is shown in Figure 8.

Results and data analysis

HVSR data quality

After downloading the data using MoHo's proprietary Grilla software, individual measurements were selected for analysis. It was observed that the recordings from the deepest part of the paleochannel had the most distinct HVSR peaks. An example of such a recording is presented in Figure 9. The example shows results from Traverse 7, site 24 (refer to Fig. 1 for location). The recording shows an acquired HVSR spectral ratio (red line) and the 95% confidence limits (grey lines; Fig. 9a). The stratigraphic peak occurs at 0.94 Hz, which, being lower than 1 Hz, indicates an impedance contrast at depth rather than a shallow regolith interface or cultural noise effect. The amplitude spectra of the three components was computed for each 20-second window via fast Fourier transform, and smoothed with a triangular 10% window (Fig. 9b). Horizontal components – north–south (green) and east–west (blue) – in the amplitude spectra are usually very similar unless there is strong anisotropy in the near surface. The vertical (purple) component dips due to resonance from trapping by underlying layers, creating an eye-like shape in the amplitude spectra (Fig. 9b). This eye-like shape in the amplitude spectra corresponds to the stratigraphic peak in the HVSR (Fig. 9). The consistency of the noise signal throughout the acquisition is shown in the time stability plot (e.g. Fig. 9c).

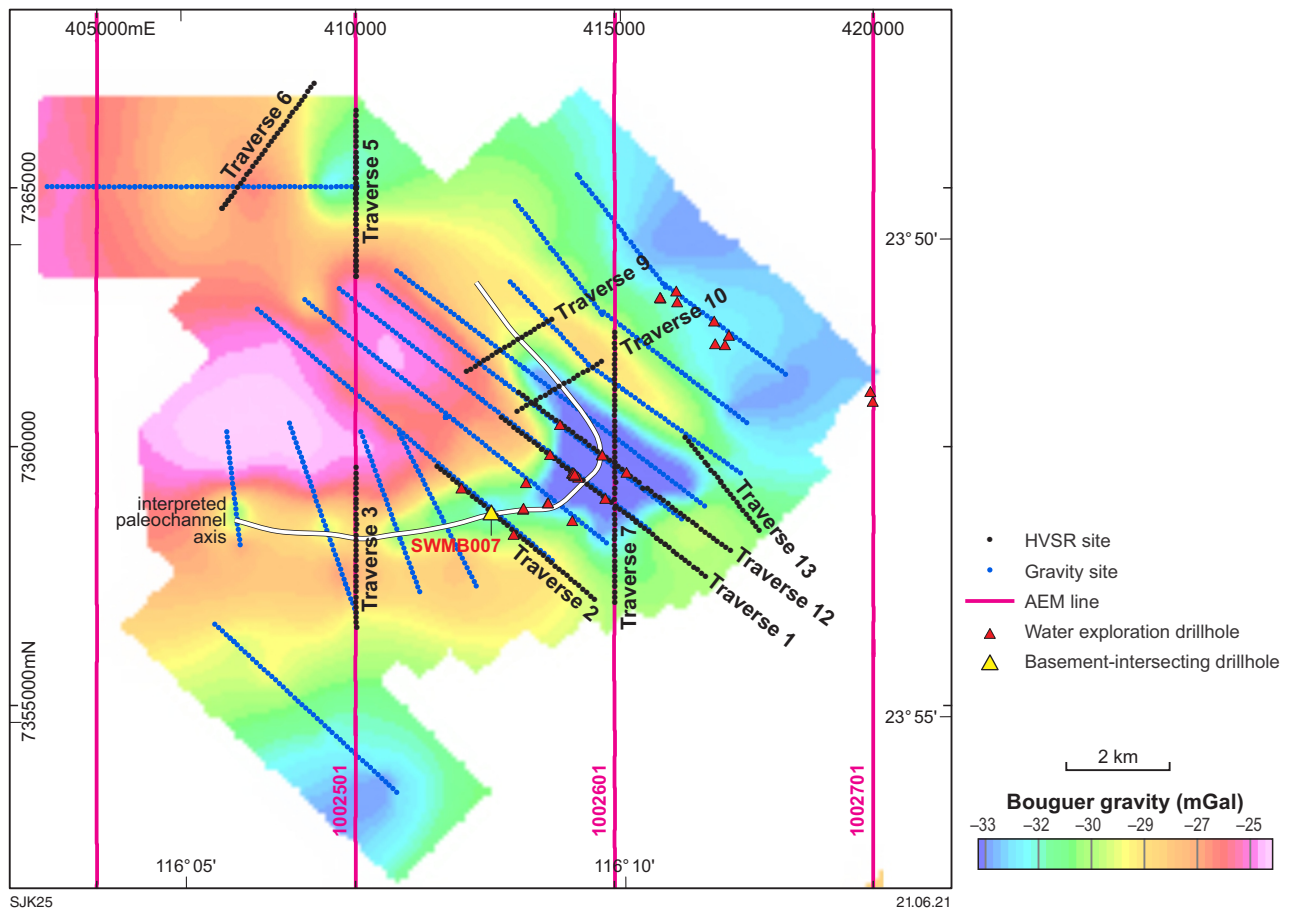


Figure 8. High-resolution Bouguer gravity data (100-m station spacing) showing the gravity low produced by the paleochannel

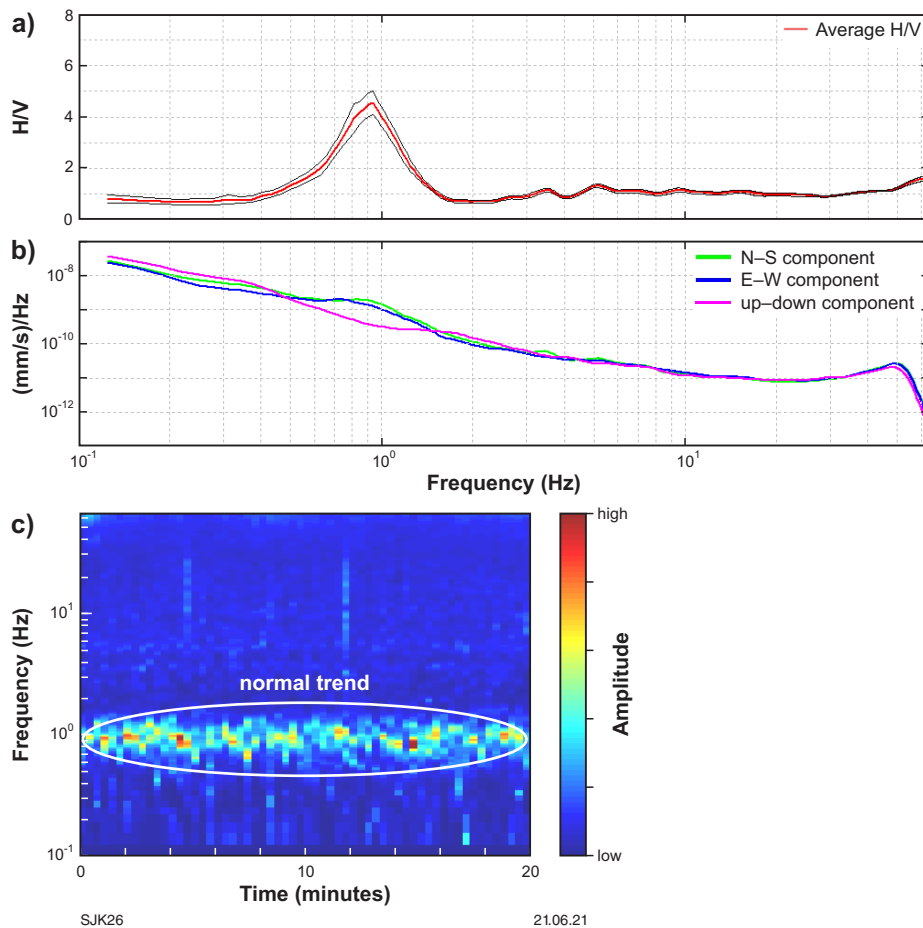


Figure 9. HVSr analysis in the proprietary Grilla software: a) HVSr spectra; b) amplitude spectra showing the horizontal and vertical components forming a distinct eye-like shape; c) stability plot of the HVSr curve during the measurement showing the amplitude of the resonance frequency over the 20-minute acquisition. Red indicates high amplitude; blue indicates low amplitude. Time is on the x-axis and frequency on the y-axis. The normal trend is shown by a white circle

A linear feature in the stability plot represents a constant, coherent noise occurring at the same frequency as the eye-like shape in the amplitude spectra and the stratigraphy peak in the HVSr (Fig. 9c) and, in this record, is referred to as the normal trend.

For some measurements, a high amplitude peak was present in the HVSr measurements but the eye-like shape in the amplitude spectra was not distinctly defined, due to weak resonance or noise disturbance (Fig. 10a). With such recordings, it was difficult to define the origin of the peak, and the smoothing was dropped from 10% to 1–5% (Micromed, 2009). By reducing the smoothing, non-stratigraphic peaks in the spectral plot appeared as thin spikes on all three spectral components and became distinctly different from the stratigraphic peaks (circled in Fig. 10b) (Micromed, 2009). This also shows that the high-frequency peak in this case was a non-stratigraphic recording.

At some sites, shallow, high-frequency, high-amplitude HVSr values were interpreted to be the result of an acoustic impedance contrast in the regolith (Fig. 11), possibly a sand/clay layer or calcrete, which is intersected in some drillcores (see Fig. 3) (Jefferson and McDougall, 2019).

Based on previous studies (Meyers, 2017; Jakica, 2018), the lower frequency peaks in multiple-frequency-peak spectra are interpreted to represent the bedrock (Fig. 7). Higher frequency peaks are interpreted to represent shallow regolith interfaces (Figs 7, 11). Interpreted regolith interfaces are present at several sites (e.g. Fig. 11) but do not extend throughout the paleochannel. The trends presented in Figure 11 are a good example of multiple frequency peaks where the high-frequency peak was distinct and easily defined. Most of the high-frequency peaks in the multiple-frequency spectra recordings appeared as broad peaks that were affected by noise. In such cases, it was not possible to determine if the broad peak resulted from an acoustic impedance contrast within the regolith or from transient noise. Therefore, due to the limited extent of multi-frequency peaks and the difficulty of distinguishing the high-frequency stratigraphic peaks from the transient/white noise, the interfaces within the regolith were not mapped. Measurements above shallow basement produced broad high-frequency HVSr peaks, with large variations in amplitude between the horizontal and vertical components over the whole frequency range (e.g. Fig. 12). These measurements have been processed with caution and their interpreted depths are less reliable.

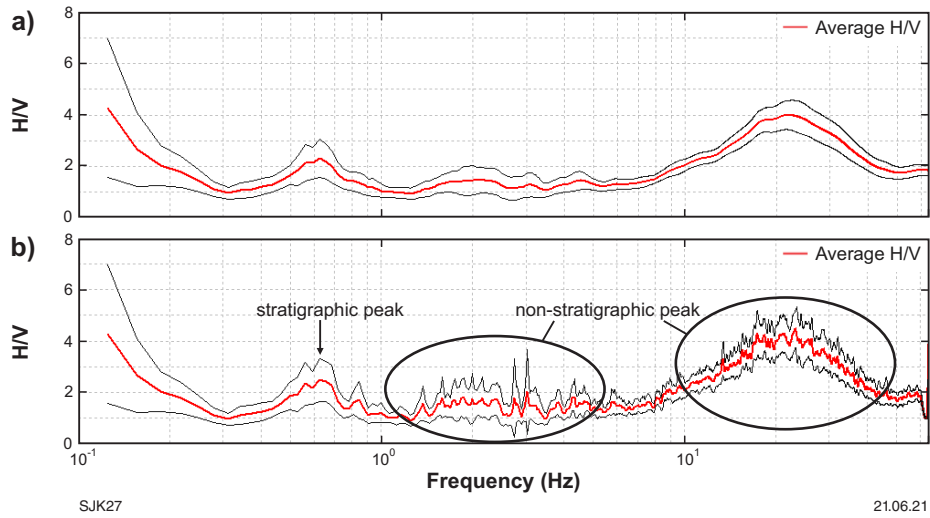


Figure 10. H/V spectral ratio with a) 10% smoothing; b) 1% smoothing. Decreased smoothing makes it possible to distinguish between the stratigraphic and non-stratigraphic peaks in the multiple-frequency-peak HVSR plot

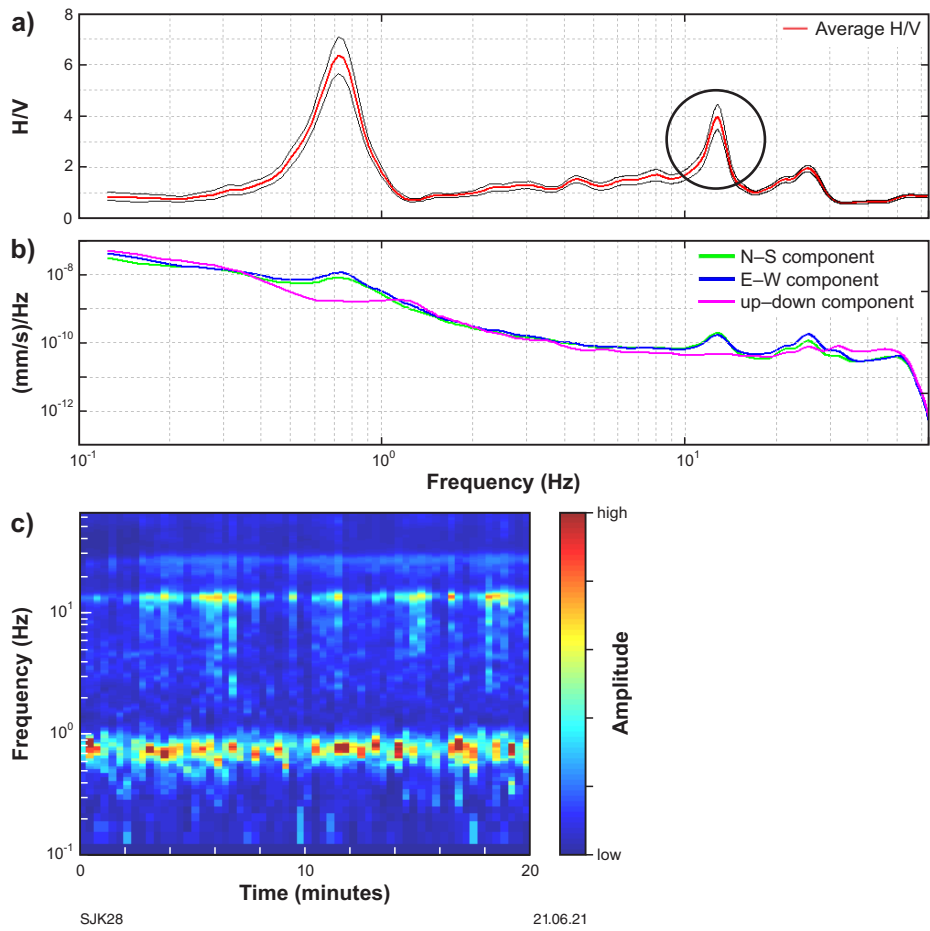


Figure 11. Multi-peak HVSR recording at Traverse 1, site 19, where: a) both low- and high-frequency (circled black) peaks are stratigraphic peaks; b) eye-like shape of stratigraphic peaks from a) is clearly defined; c) two normal trends in the stability plot are also confirming the two stratigraphic peaks

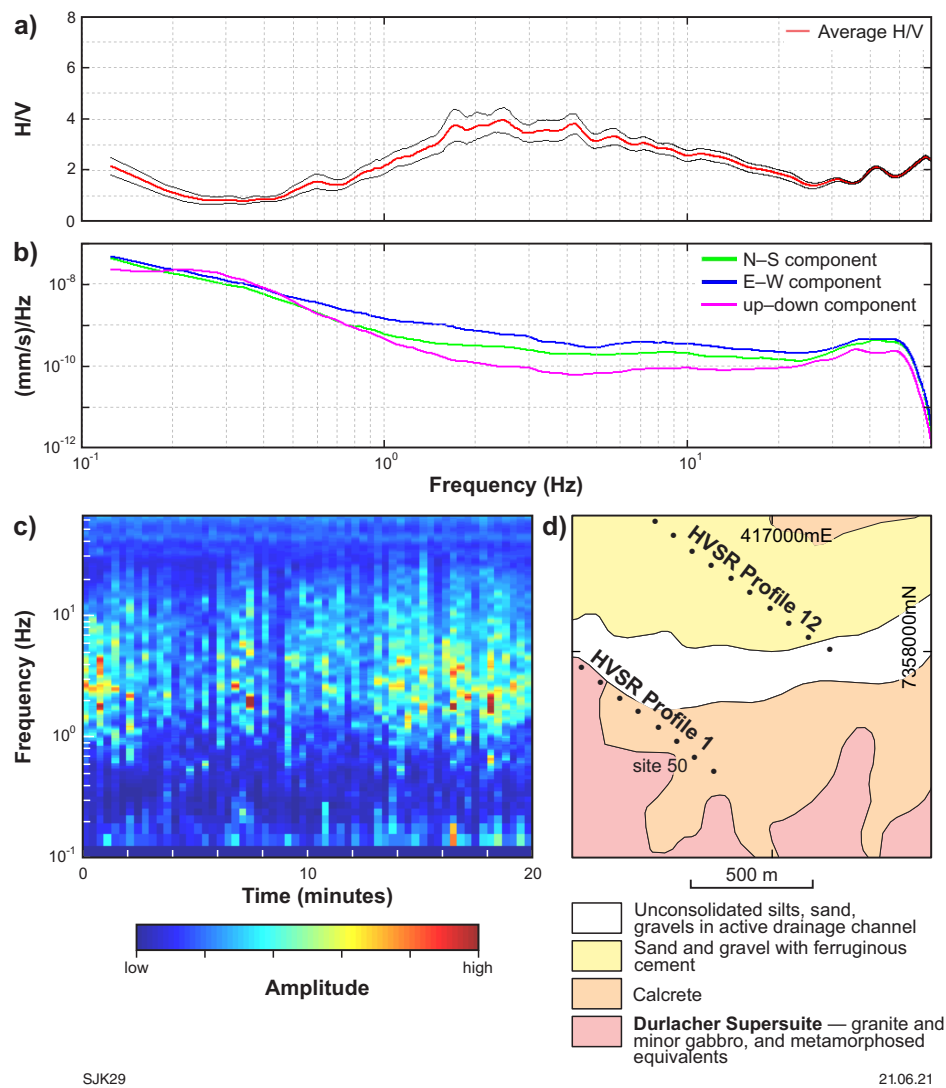


Figure 12. Shallow-basement HVSR recording showing a broad frequency peak in a); b) amplitude spectra of the broad HVSR curve; c) stability plot of the recording; d) geology map of the site area. The recording is from seismic Traverse 1, site 50. The geology map suggests shallow regolith in the area

At several sites, stratigraphic peaks with two maxima were observed in HVSR spectra (e.g. Traverse 7, site 22; Fig. 13). The two maxima possibly indicate a thin layer of material, such as weathered bedrock, at the regolith–bedrock interface. At sites where stratigraphic peaks have two maxima, the frequency of the middle of the two peaks, as indicated by the plus sign in Figure 13, was used to calculate the depth to basement (Fig. 13). It is assumed here that those two peaks are representative of a broader single curve (dashed line in Fig. 13a), hence the middle of the two peaks represents the peak of a single curve.

Transient and/or near-white noise (e.g. herd of cattle galloping by, wind or other acoustic noise) was recognized by a signal that strongly deviated from the normal trend. Transient noise appears as dispersed warm colors in the stability plot (Fig. 14a). Most of the noise recorded in this study was high frequency in character and interpreted to be due to wind (such as for Fig. 14a). Sometimes the data quality was improved by removing the noise from the readings. An HVSR stability plot before noise removal is presented in Figure 14a, where the normal trend is a

maximum HVSR between 0.8 and 1.01 Hz while the noisy windows show dispersed warm colors away from the normal trend at higher frequencies. The noisy data were excluded from the analysis by selecting for analysis only certain windows as shown in Figure 14b.

In some recordings, the stratigraphic peak was masked by high-amplitude transient noise that could not be removed (Fig. 15a). In such cases, the stratigraphic peak was defined based on the frequency of stratigraphic peaks at neighbouring sites. For example, along Traverse 2, a distinct stratigraphic peak at station 10 (circled; Fig. 15b) was used to define a stratigraphic peak masked by noise 200 m away at station 8 (circled; Fig. 15a).

For some measurements, the N–S component in the amplitude spectra deviated from the E–W component forming an L-shaped pattern (Fig. 16a). This could have been caused by either a faulty instrument with a non-responsive N–S component, or poor coupling. It has been found that one Tromino unit was faulty, causing the N–S component to deviate.

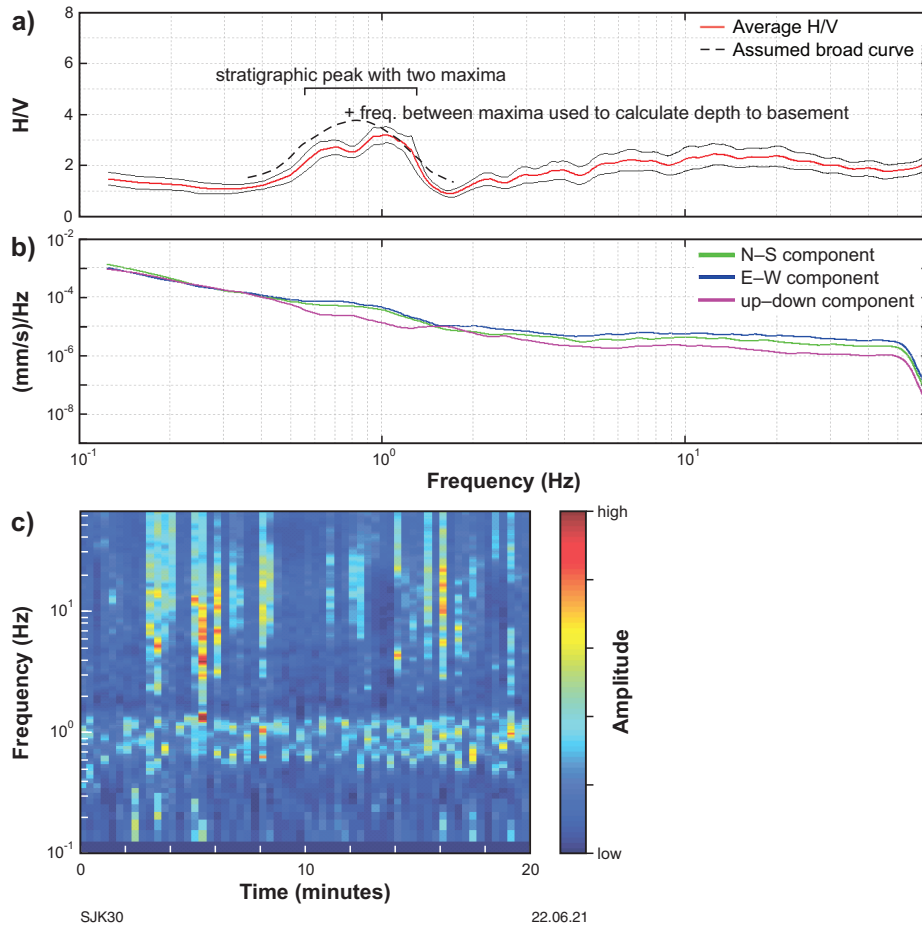


Figure 13. An example of a two-maxima stratigraphic peak recording from Traverse 7, site 22. The frequency of the middle of the two peaks was used to calculate the depth to basement

At some pisolith-rich sites, measurements repeated to address this issue with two different Tromino units showed the same deviation of the N–S component. It was observed that at these sites the thicker custom-made spikes did not produce the best coupling with the ground and the use of the longer, thinner MoHo spikes improved the recording quality. Where the recording quality was not improved, the N–S component was ignored and the E–W component was used to define the frequency peak in the HVSR spectra ratio (Fig. 16b).

Velocity calibration at drillhole

Interpretation of HVSR measurements using Grilla software involves fitting a synthetic curve to the measured frequency peaks in the HVSR spectrum (Fig. 17a,b). This was carried out by constraining a velocity–depth model using Equation 1 and HVSR readings at drillhole SWMB007, where the depth to the basement was known (Fig. 17c,d). The modelled velocity of 290 m/s was used at each subsequent HVSR measurement to estimate the depth to basement, i.e. depth of the Yangibana paleochannel. A limitation of this study is that the shear-wave velocity of the regolith package has only been calculated at one location, SWMB007. The use of this constant velocity throughout the study area is a simplification but, without more basement-intersecting holes, this is unavoidable.

Data visualization

HVSR vs elevation

To visualize HVSR data, HVSR values have been normalized and frequencies converted to elevations. HVSR values at each site have been normalized using min–max normalization:

$$x^1 = (x - \min(x)) / (\max(x) - \min(x))$$

where: x^1 = normalized value
 x = original value

Normalization transforms the HVSR amplitudes, which can vary a lot between sites, to a range between 0 and 1. This makes the HVSR values comparable between sites, although in some cases enhances noise.

Measured frequencies were then converted to elevations. For each measurement, HVSR data were recorded at 2048 different frequencies. These frequencies (f_z) were converted to thickness (h) assuming a velocity (V_s) of 290 m/s and using the equation $f_z = (V_s/4h)$. The thickness was then subtracted from the elevation of the site to give the depth of the data point. Normalized HVSR values and basement peaks for the ten traverses are shown in Figure 18.

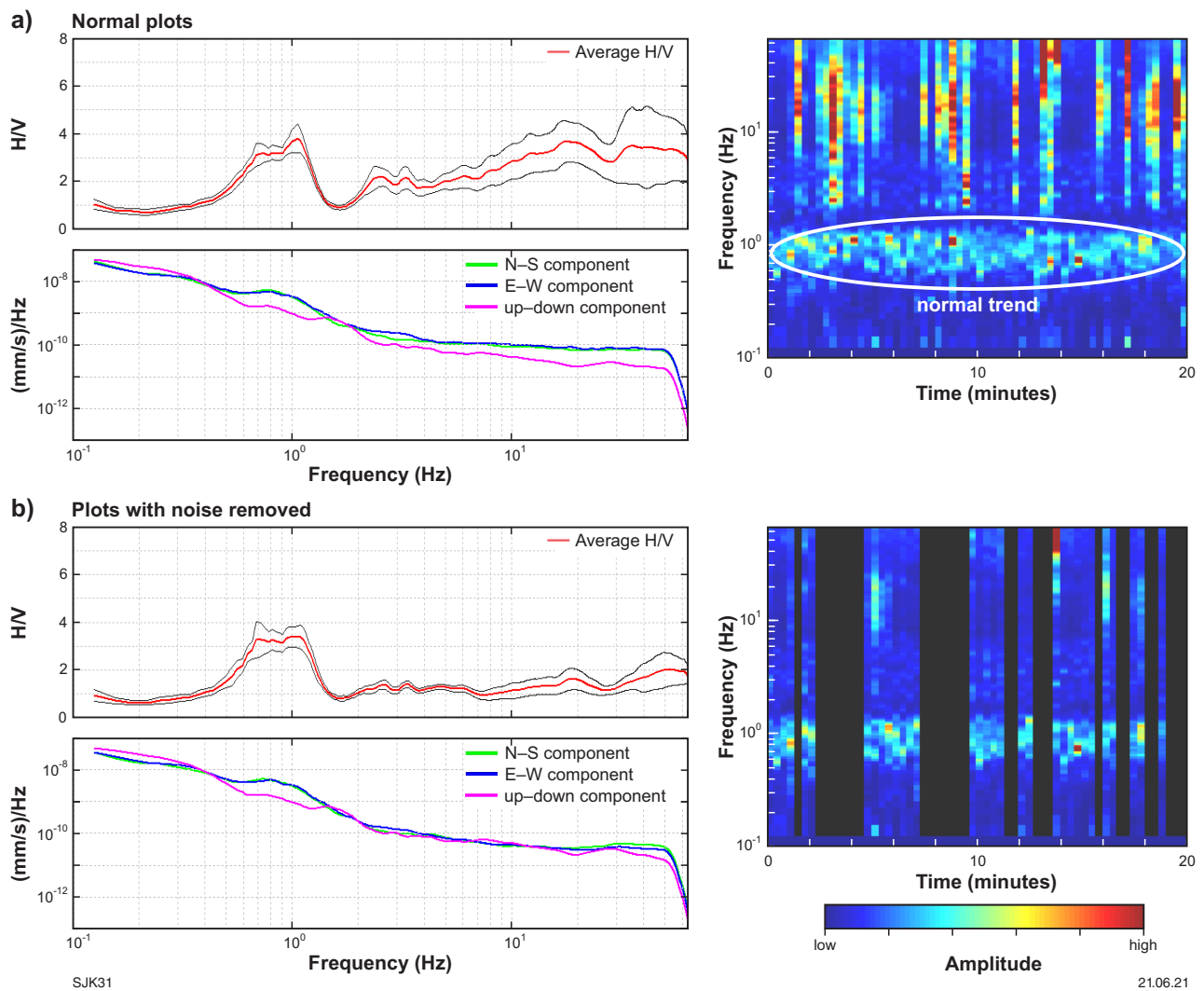


Figure 14. Effects of noise removal. HVSr recording from Traverse 1, site 27: a) before and b) after trace cleaning

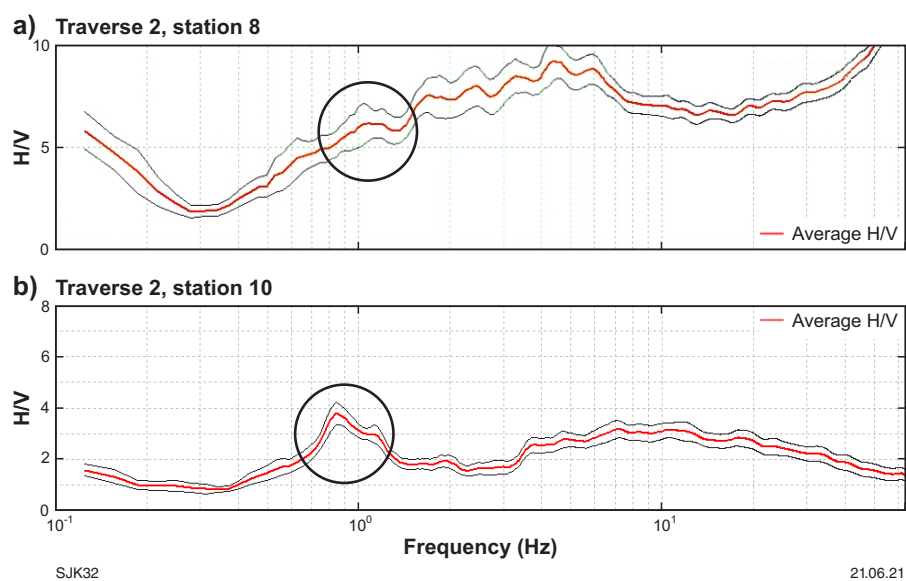


Figure 15. Extrapolating from a near-by site: the peak at station 8 shown in a) has been determined based on the peak at station 10 shown in b). Station 10 is only 200 m away from station 8. The higher frequency peaks are noise and were ignored

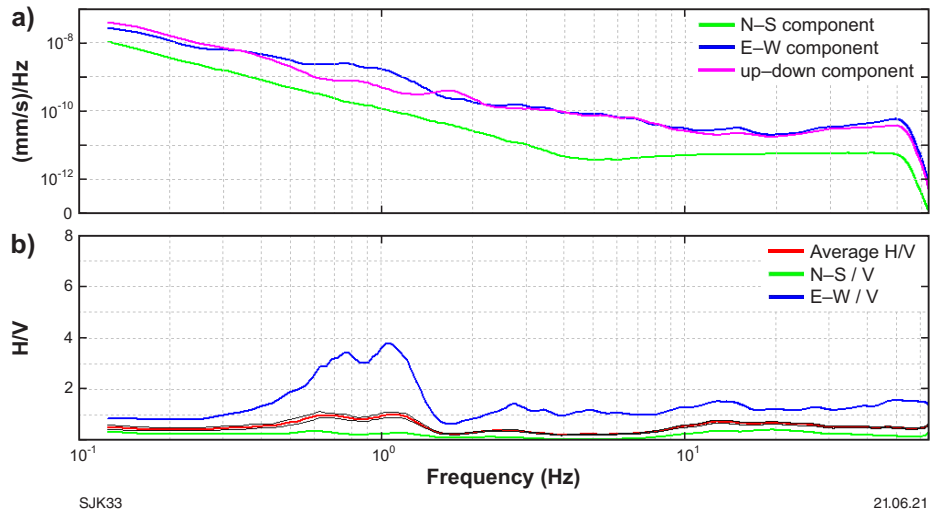


Figure 16. HVSr recording where north-south component is not responsive: a) north-south component deviates in an L-shaped pattern in the amplitude spectra; b) east-west component used to define the frequency peak in the H/V spectral ratio

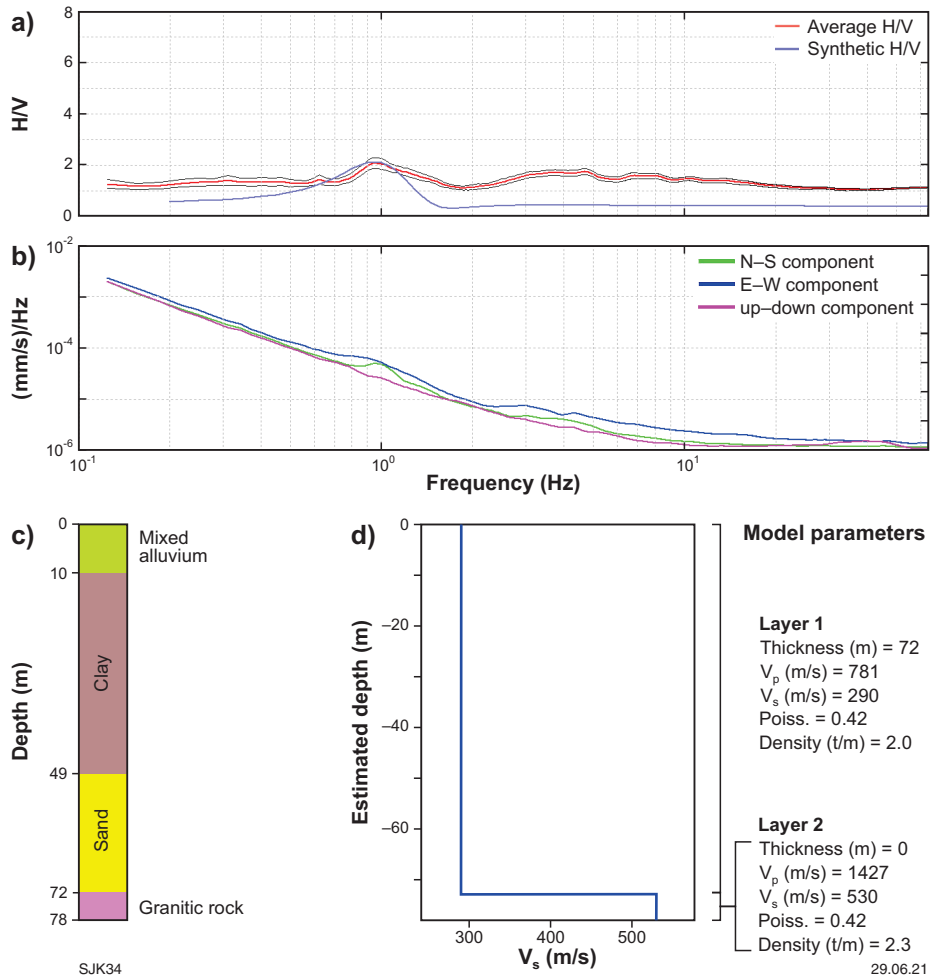


Figure 17. V_{s1} estimation at drillhole SWMB007: a) observed (red and black) and synthetic (blue) H/V spectra; b) amplitude spectra; c) logged geology at SWMB007; d) velocity model and model parameters, including the V_{s1} used to produce the synthetic H/V spectra in a)

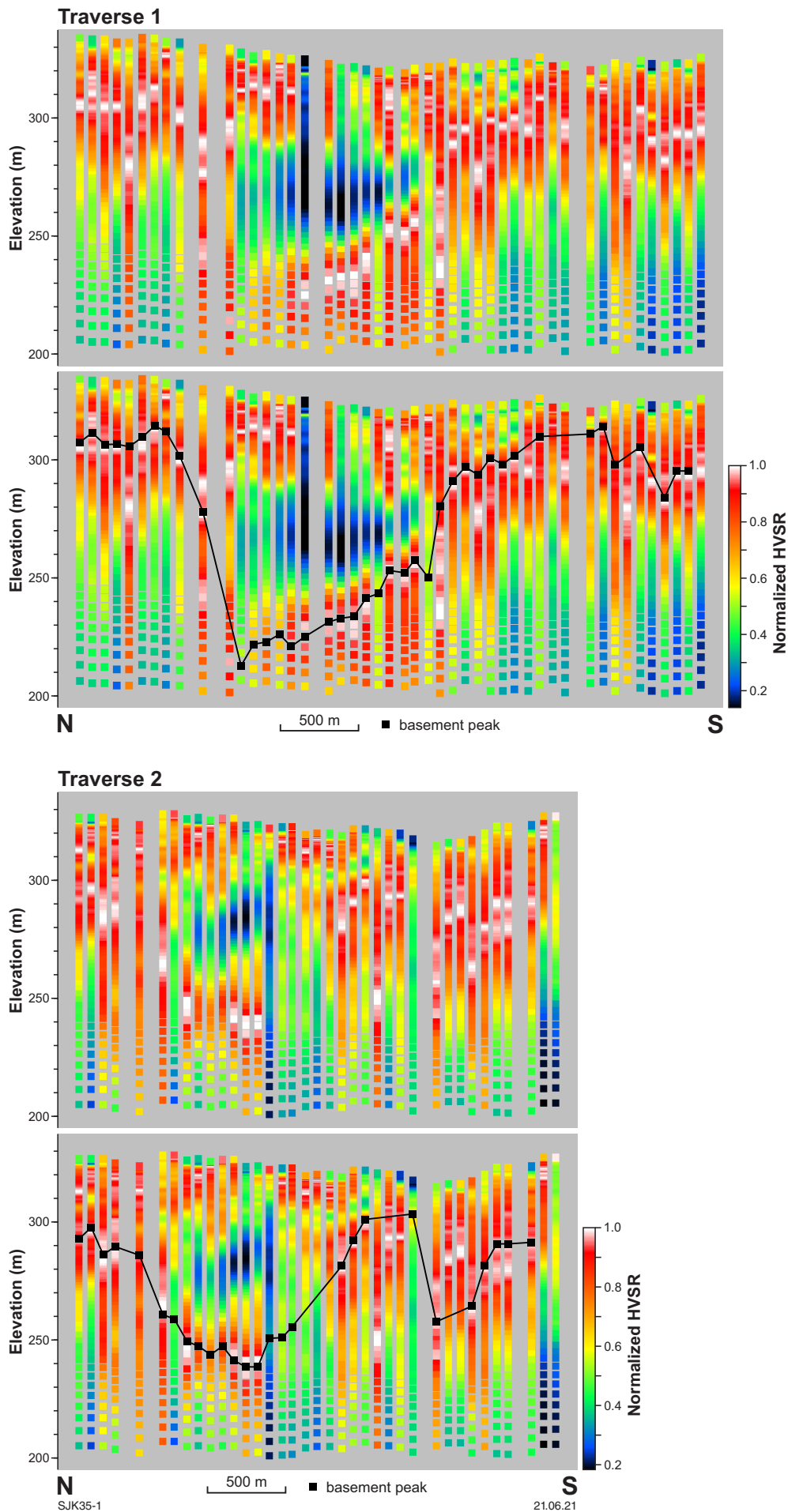


Figure 18. Normalized HVSR values for all 10 profiles plotted in 3D. The black line indicates interpreted depth to the basement. Traverse 13 is outside the margins of the interpreted paleochannel and shows shallow subcropping to outcropping basement (black squares). Vertical exaggeration is 15x

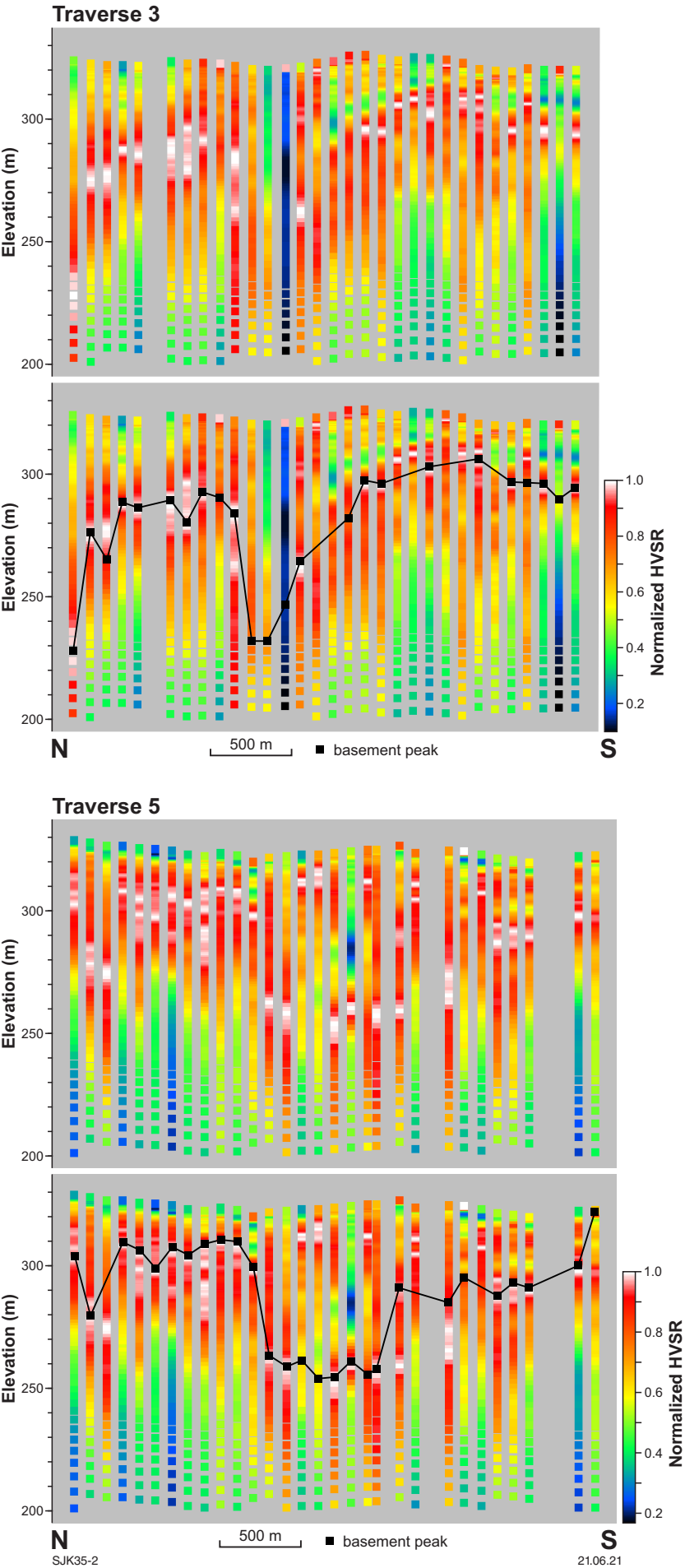


Figure 18. continued

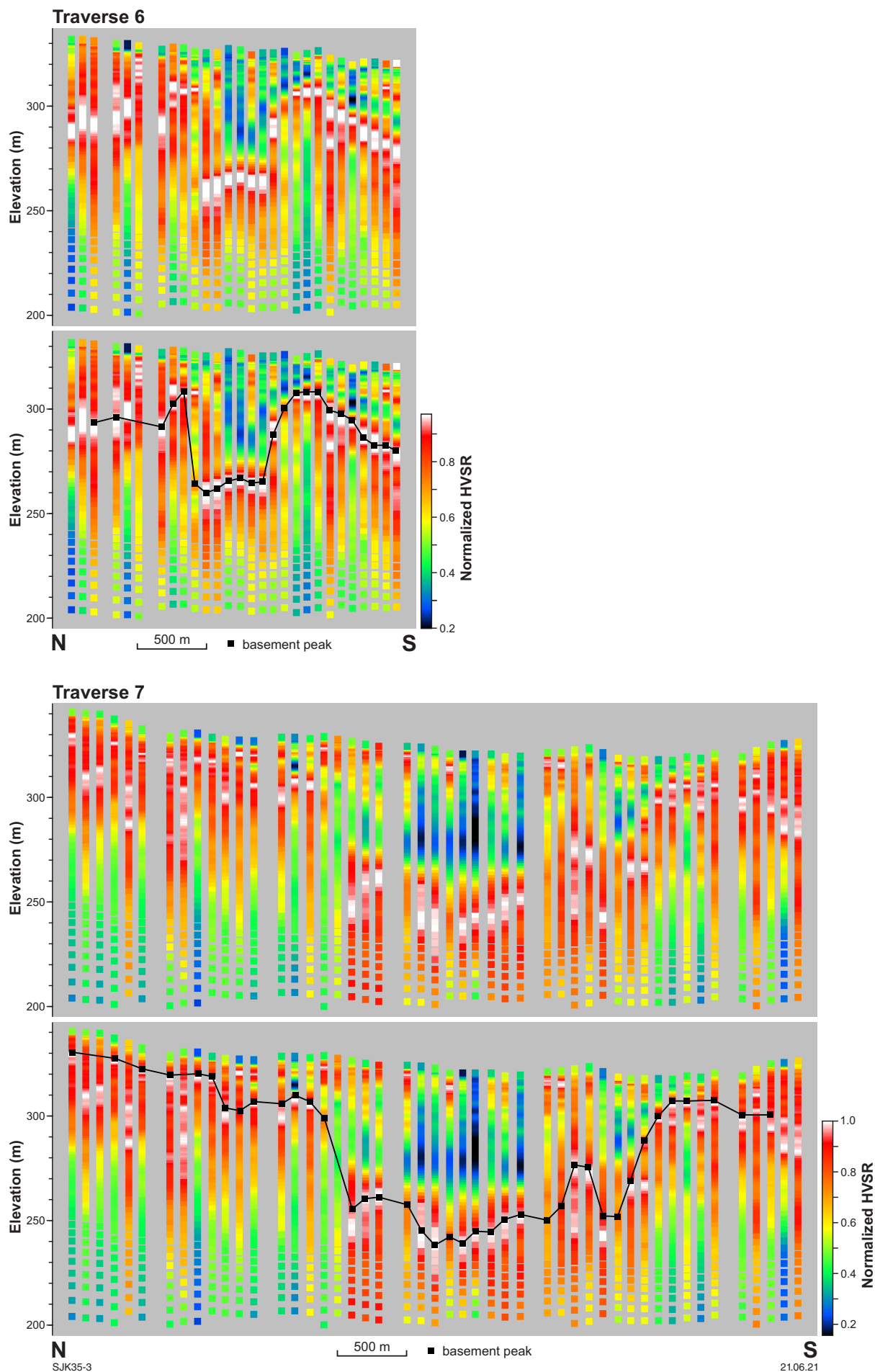


Figure 18. continued

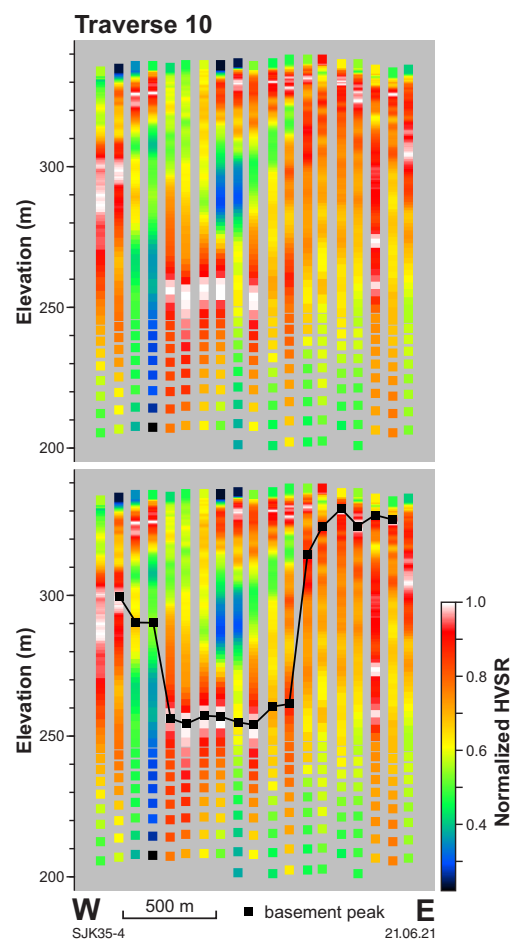
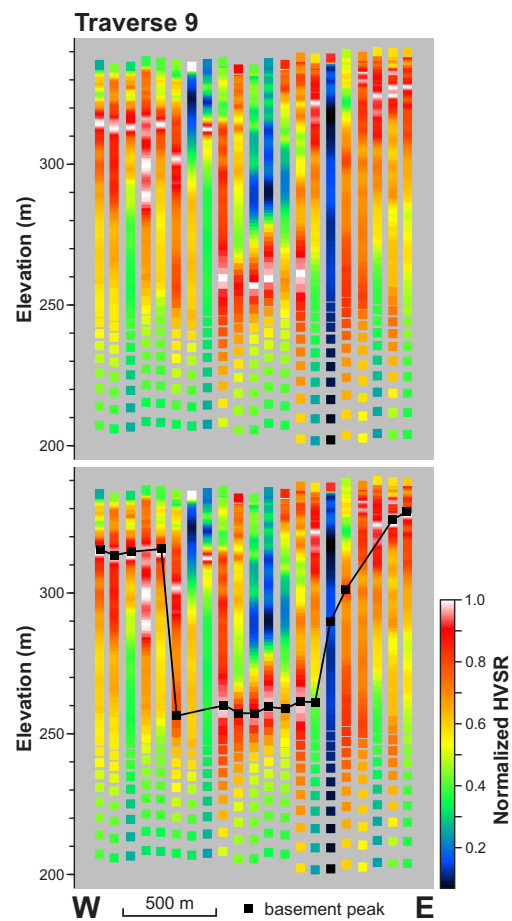


Figure 18. continued

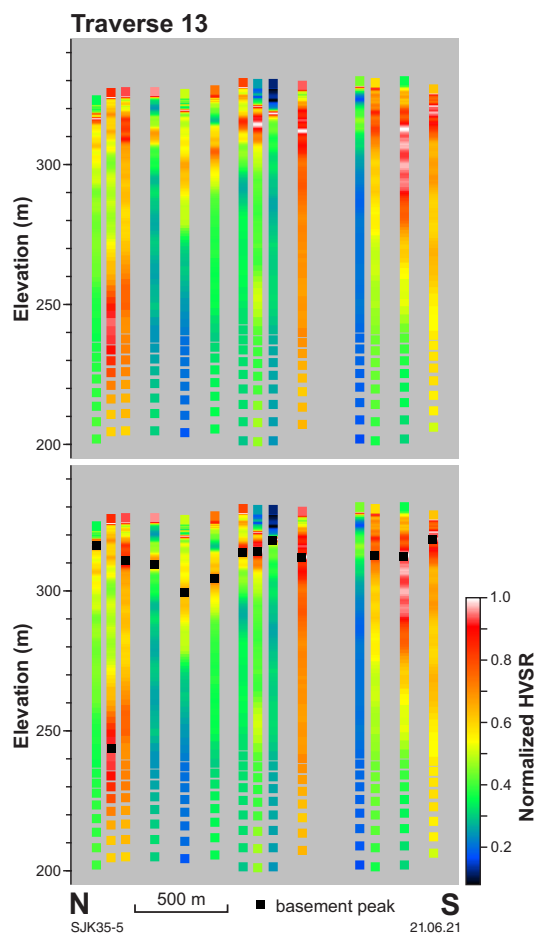
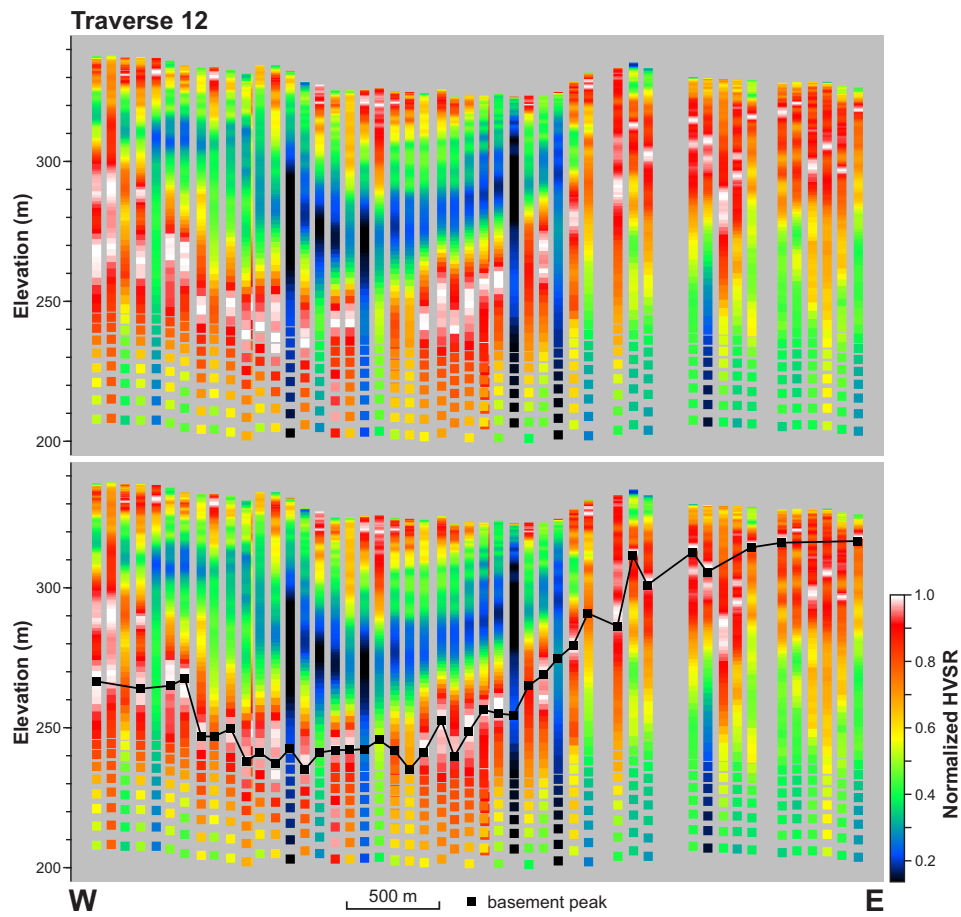


Figure 18. continued

At most sites, the basement peak corresponds to the highest normalized HVSR value. The interpreted depth of the paleochannel is marked with black lines in Figure 18. Note that Traverse 13 runs outside the margins of the interpreted paleochannel. This traverse was designed to check if the paleochannel extends further to the east. The highest normalized values (black squares along Traverse 13; Fig. 18) are indicative of a very shallow basement. This is concordant with the geology map, suggesting a thin layer of calcrete overlying igneous rocks of the Durlacher Supersuite (Figs 2, 18). The deeper basement on the north side of the traverse is indicative of thick transported material from the recent alluvium infill.

3D depth to basement surface

The 275 depth-to-basement interpretations from HVSR data were imported as 3D points into 3D modelling software GOCAD v. 19. In GOCAD, a surface representing depth to basement was produced by interpolation, using the Discrete Smooth Interpolator (DSI), to smoothly fit a surface to the HVSR depths that represent the depth of the paleochannel. Due to the larger distance between Profiles 5 and 9, compared to other profiles, the dataset was interpolated in two parts (Fig. 19a,b). As an alternative, several artificial data points were added between Profiles 5 and 9, where no data were available, and the dataset was interpolated to produce one surface representing the base of the paleochannel (Fig. 19c).

Paleochannel geometry

When viewing all available depths recovered from HVSR, these HVSR data show a meandering paleochannel. The broadest and deepest (116 m) part of the paleochannel is in the east where the channel changes orientation (Traverse 1, site 14; Fig. 1). Traverse 1 HVSR data suggest the channel is asymmetrical. Unusually, the inner channel, where deposition occurs, is steepest and the outer channel, where erosion occurs, is shallower (Fig. 18). Away from the meander, the channel is narrower, shallower and symmetrical (Fig. 18). The northern channel has a box-shaped geometry and a maximum depth of ~50 m (Traverses 10, 9, 6 and 5; Fig. 18). The southern channel is narrower and also has a maximum depth of ~50 m (Traverse 3; Fig. 18).

Comparison of HVSR to other geophysical methods

2.5D AEM inversion

The 2.5D inversion profiles for AEM flight lines 1002501 and 1002601 in the study area are presented in Figure 20. Using the drillhole data available and company potential-field data, Hastings Metals geologists (Jefferson and McDougall, 2019) have interpreted the axis of the paleochannel to trend northwesterly and change direction to westerly trending in the east near AEM line 1002601 (white line in Figs 8, 21a).

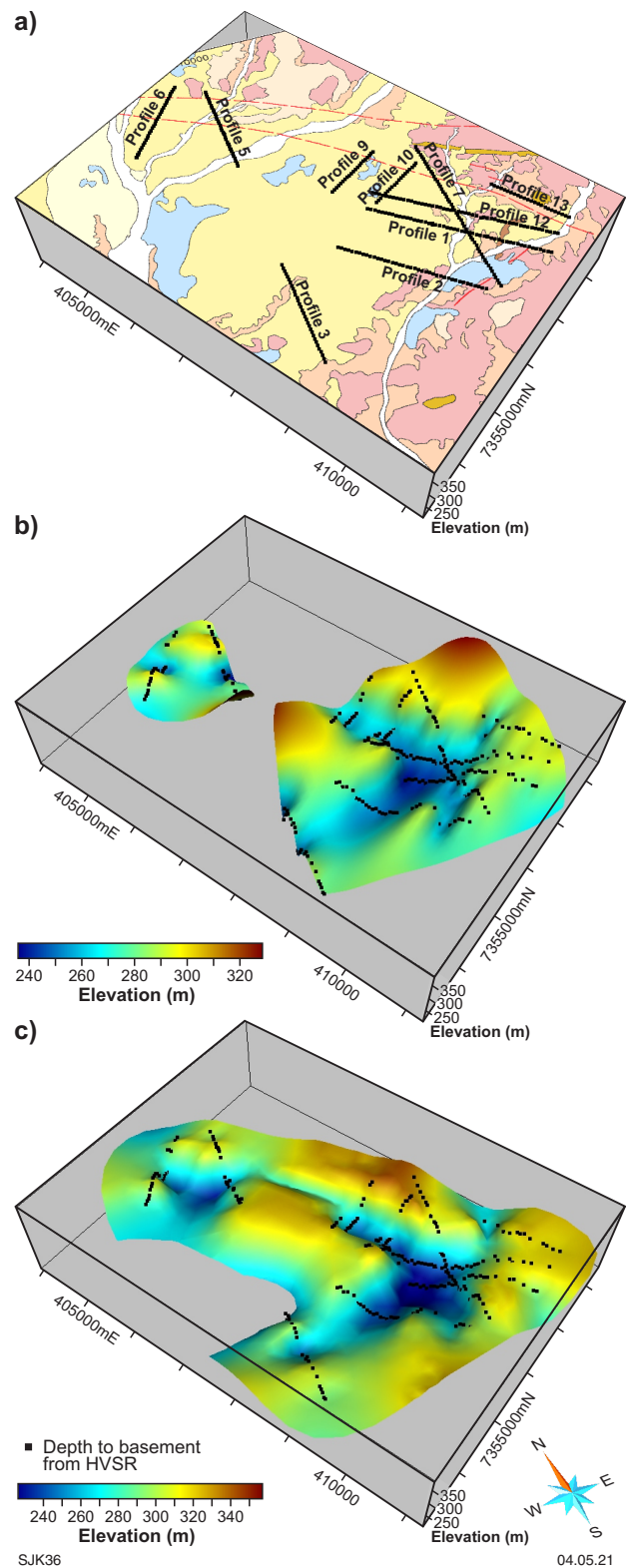


Figure 19. A 3D representation of the basement surface: a) geology image showing the orientation of the HVSR traverses; b) data interpolated in two parts; c) data interpolated to produce one 3D surface that shows the geometry of the paleochannel

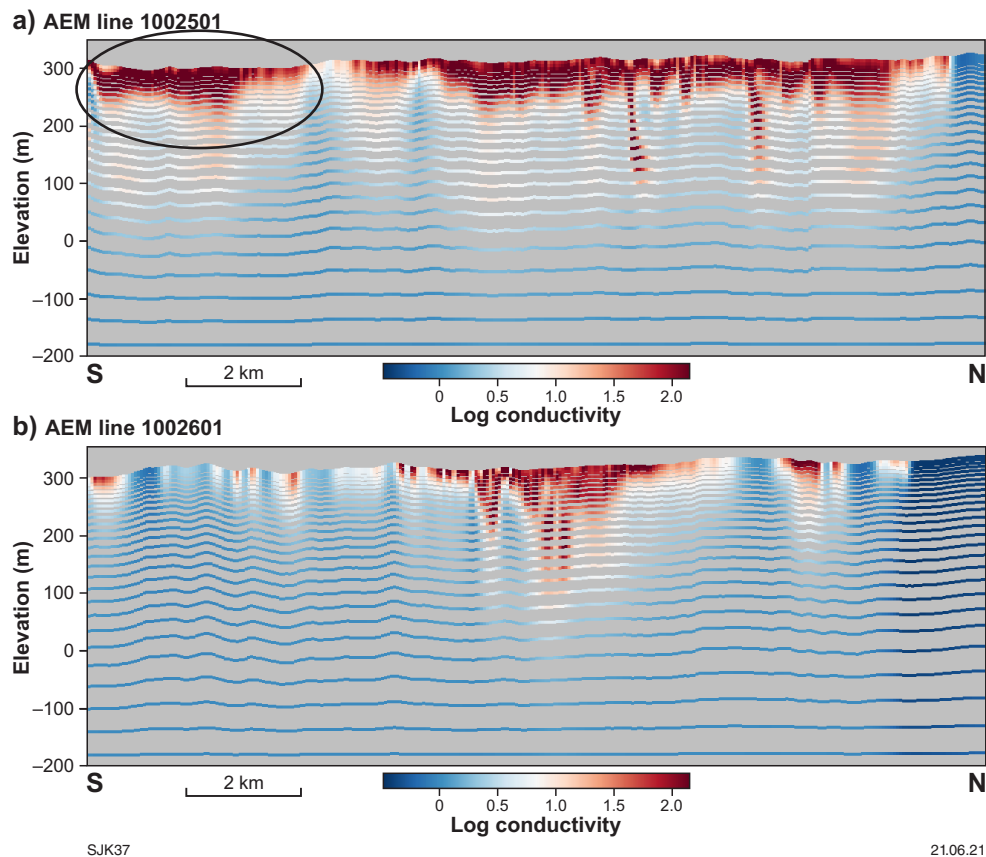


Figure 20. The 2.5D inversion profiles of the Capricorn 2013 AEM lines in the study area: a) AEM line 1002501 (black circle indicates the southern part of the reflective anomaly located outside the paleochannel axis); b) AEM line 1002601. Vertical exaggeration is 10x

Figure 21b shows the drillhole data in relation to the 2.5D conductivity model along AEM line 1002601. The drillhole data suggest that the conductive anomaly is related to the Yangibana paleochannel comprised of clays and sandy clays that host the groundwater while the non-conductive materials are sands or granitic basement (Figs 21b, 22). An excellent agreement between the interpreted paleochannel axis, magnetic component in 1VD RTP aeromagnetic imagery and highly conductive anomaly in 2.5D AEM all support the paleochannel geometry recovered from the HVSR component of this study (Fig. 21).

There are two conductive anomalies present along the line 1002501 (Fig. 20). The anomaly in the southern part of the line lies outside the interpreted paleochannel axis (circled in black in Fig. 20; feature 1 in Fig. 22a). The geology map and the gravity data indicate that this anomaly is related to the present-day transported alluvium and sheetwash regolith material in the area (Fig. 22). A non-conductive area separating the two conductive anomalies along the line 1002501 represents the outcropping Durlacher Supersuite (feature 2 in Fig. 22a). The conductive anomaly in the northern part of the AEM line can be interpreted as transported alluvium regolith and/or the Yangibana paleochannel. The shallow conductive anomaly in the middle part of the AEM line is coincident with the gravity high and magnetic low, which suggests it is most likely transported regolith overlaying the shallow basement (feature 3 in Fig. 22a). If the only available data were the potential-field and AEM profiles, it would be challenging to distinguish what part of the AEM conductive

layer represents the paleochannel and what is the depth and also overall geometry of the paleochannel.

To validate the Yangibana paleochannel geometry mapped with AEM, AEM and potential-field data were analysed in conjunction with the passive seismic results. Three passive seismic traverses were designed to run along the two AEM lines (Fig. 1). Traverses 3 and 5 run along AEM line 1002501, while Traverse 7 runs along line 1002601 (Fig. 1). The interpreted base of the paleochannel obtained from HVSR analysis is compared against the conductivity section from 2.5D inversion of AEM data and presented in Figure 23.

Comparison of the passive seismic and AEM data along Traverse 7 shows that the depth to basement calculated from HVSR data is broadly similar to the depth to basement from AEM. For example, a separate smaller channel at the northern margin of the paleochannel is imaged in both passive seismic and AEM (labelled 1 in Fig. 23a,b). However, one of the major differences is the maximum depth of the paleochannel. Passive seismic predicts a shallower maximum (~116 m) than AEM (~170 m) (labelled 2 in Fig. 23a,b) along AEM line 1002601. This may be a result of the inversion algorithm used but may also represent an overestimation of the depth due to challenges in recovering the conductivity of the layer beneath the conductive regolith layer overlying the paleochannel. Another reason for the discrepancy might be the use of a single V_s constraint from drilling to estimate the paleochannel depths from the HVSR data.

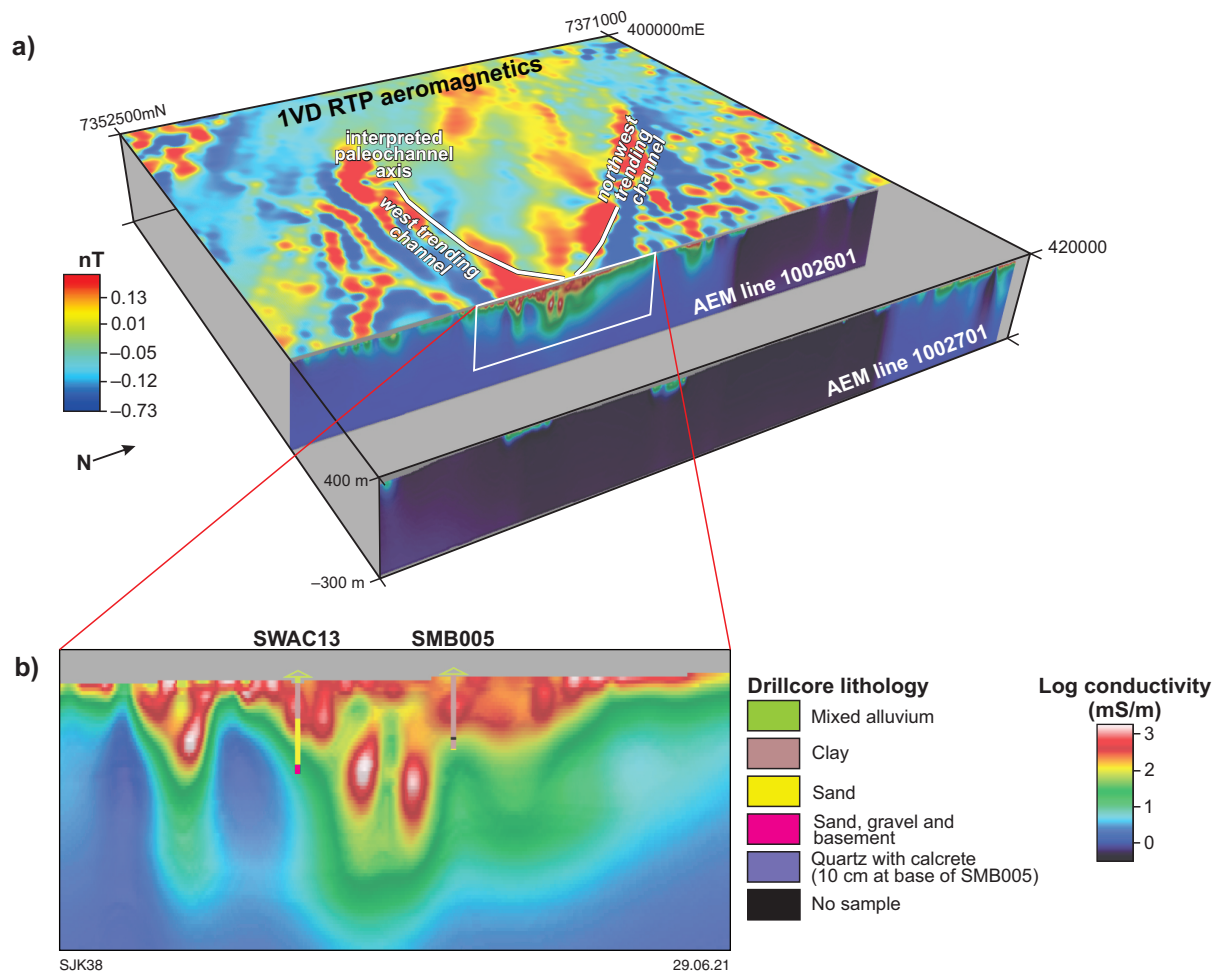


Figure 21. AEM and aeromagnetic data: a) 3D view of conductivity section along AEM line 1002601 and 1VD RTP aeromagnetic data; b) drilling data projected to AEM line 1002601

The interpreted base depths of the paleochannel from Traverses 3 and 5, along AEM line 1002501, clearly distinguish its geometry from the conductive regolith layer (Fig. 23c,d). The passive seismic traverses do not extend across the entire conductive anomaly (black circle in Fig. 23d). Nevertheless, the passive seismic results immediately before the gap in data still suggest that the base of the channel shallows. This further suggests that the AEM conductivity within the high-gravity zone (Figs 22, 23d) is representative of a transported regolith unit.

Gravity

HVSR Traverses 1, 2 and 12 follow parts of three gravity profiles (Fig. 8), making it possible to compare the results from these two methods (Fig. 24a–c). Along these profiles, the depth-to-basement values, calculated from HVSR data, have been compared to Bouguer gravity data. High-resolution Bouguer gravity data show the paleochannel as a gravity low, produced by an increased thickness of low-density channel fill (Fig. 24). Along profiles 1, 2 and 12, the gravity low produced by the paleochannel has a similar geometry to the depth of the paleochannel from HVSR data (Fig. 24). The HVSR data are generally more scattered than the Bouguer gravity data, particularly at the southeastern

ends of Profiles 1, 2 and 12, where measurements were made above shallow bedrock (circled in Fig. 24a–c). Both HVSR and gravity produce similar models of the depth of the paleochannel, although here the depth to basement has been calculated from HVSR data rather than gravity data. This is not surprising since the HVSR method is based on acoustic impedance contrasts (which are the product of shear-wave velocity and density) and the gravity method is based on density contrasts. This study suggests that either gravity or HVSR could be used to produce a model of the depth to basement, or that these methods could be used together to produce a robust model.

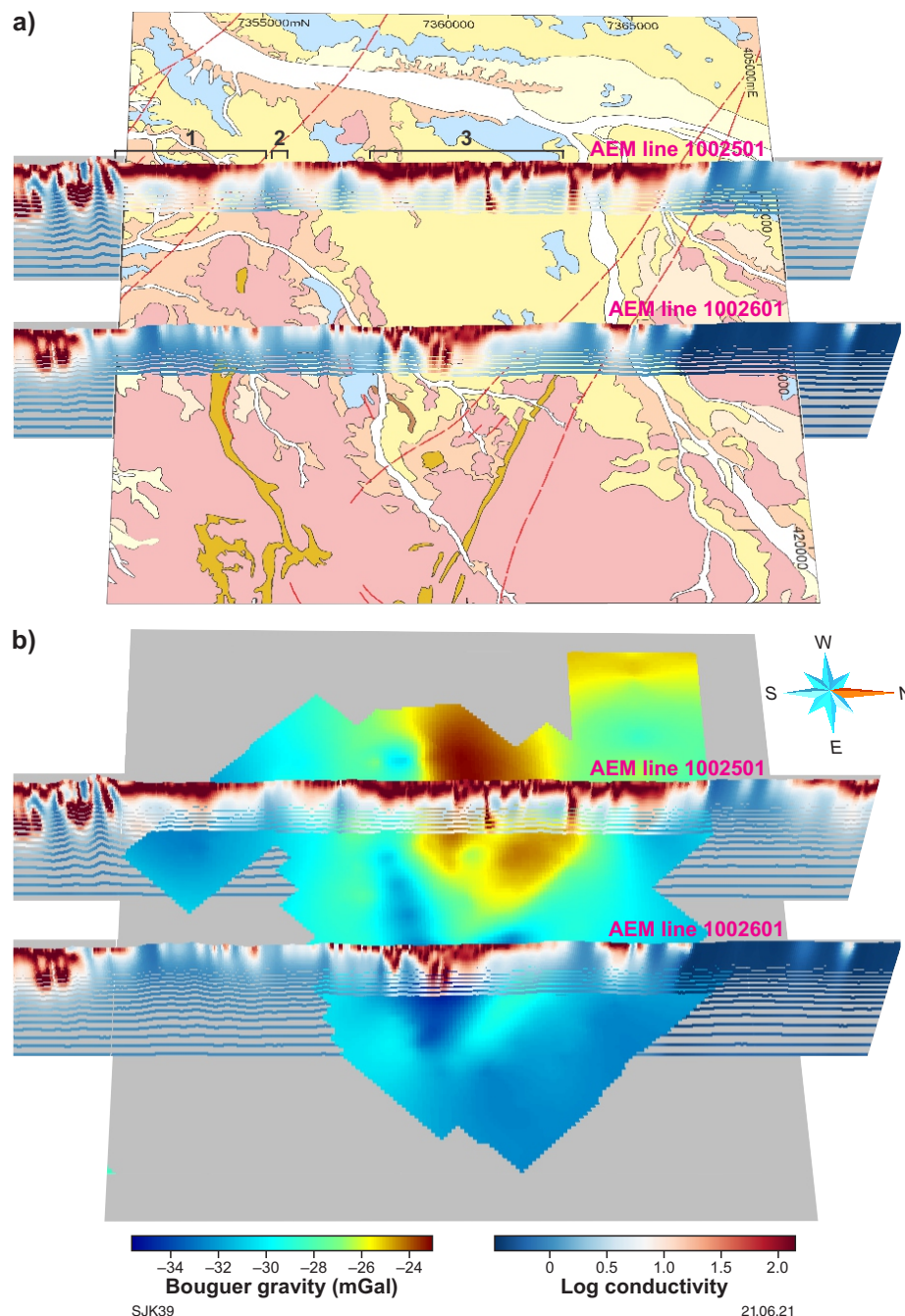
Conclusions

In this study, multiple geophysical datasets, but only passive seismic HVSR data, were used to produce a 3D model of the Yangibana paleochannel, a water exploration target, in the Gascoyne Province. The acquisition and interpretation of passive seismic data from 10 traverses provided an estimate of the 3D geometry of the paleochannel, which is equivalent to the depth to crystalline basement. In this study, the results from the HVSR data are found to be consistent with results from AEM, gravity and aeromagnetic surveys.

HVSR data show the Yangibana paleochannel has an orientation from northwesterly trending in the north of the study area to westerly trending in the south, with a maximum estimated depth of ~116 m, observed at Traverse 1, site 14, where the channel changes orientation.

Results from the HVSR data showed a good correlation with conductivity models from 2.5D inversion of 2013 Capricorn TEMPEST regional AEM data. In this study, AEM and passive seismic methods were

complementary for mapping paleochannel geometry. Passive seismic acquisition is cost-effective and rapid for small-scale surveys and, at 10-km line spacing, AEM provides detailed data along but not between lines. AEM is less effective when highly conductive shallow units might mask deeper features including the base of the paleochannel. Whereas, HVSR is not as effective in regions where the impedance contrast between the basement and the cover is not distinct.



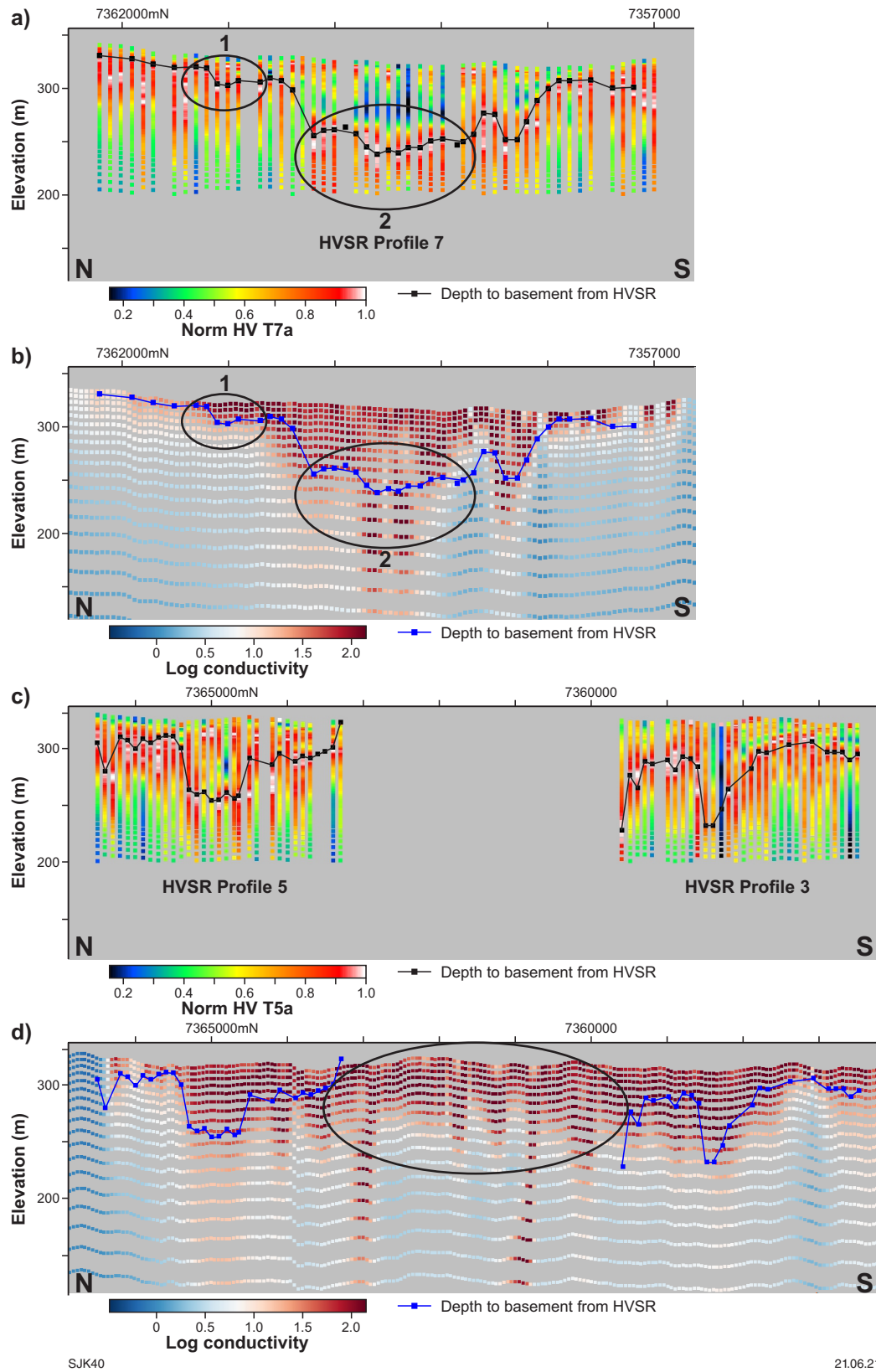


Figure 23. Normalized HVSR data and AEM data showing the base of the paleochannel interpreted from HVSR data: a) Traverse 7 HVSR data; b) AEM line 1002601 conductivity section; c) Traverses 3 and 5 HVSR data; d) AEM line 1002501 conductivity section. For more details, refer to the main text. Vertical exaggeration is 10x

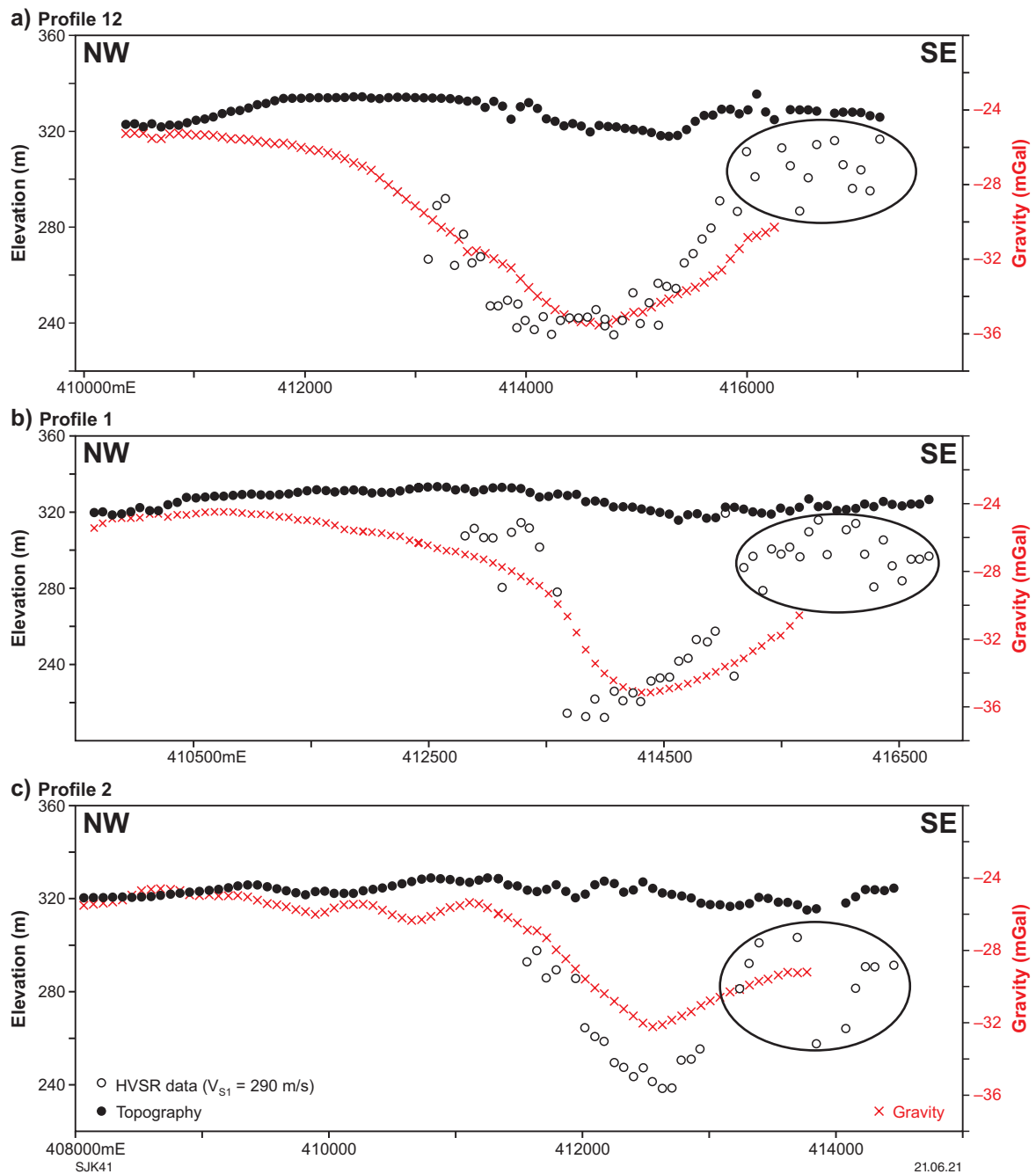


Figure 24. HVSR and gravity data shown as profiles: a) Profile 12; b) Profile 1; c) Profile 2

Calculating the depth of the paleochannel, or depth to basement, using the HVSR method requires an estimate of the shear-wave velocity of the regolith package. In this study, this velocity was estimated at the only basement-intersecting drillcore and that value applied to all measurements. In future, if more basement-intersecting cores are drilled, velocity estimates could be improved, resulting in more robust paleochannel depths. More shear-wave velocity data could also be obtained by use of active-source HVSR surveys and dispersion curve analysis.

References

- Amann, B 2018, Yangibana Gravity Survey Extension 2018: for Hastings Technology Metals, not published: Newexco, Perth, Western Australia; Report of Investigations.
- Bell, JG, Kilgour, PL, English, PM, Woodgate, MF and Lewis, SJ 2012, WASANT paleovalley map – Distribution of paleovalleys in arid and semi-arid WA-SA-NT (1:4 500 000 scale): Geoscience Australia, Geoscience Thematic Map (Geocat No. 73980).
- Border, A, Whittock, K and Coxhell, S 2017, Yangibana rare earth elements deposits, in *Australian Ore Deposits edited by GN Phillips*: Australasian Institute of Mining and Metallurgy, Monograph 32, p. 403–404.
- Castellaro, S and Mulargia, F 2009, The effect of velocity inversions on H/V: *Journal of Pure and Applied Geophysics*, v. 166, p. 567–592, doi:10.1007/s00024-009-0474-5.
- CGG 2013, TEMPEST Geophysical Survey, Capricorn Regional Survey, Western Australia, in *Geological Survey of Western Australia Airborne Geophysics database, MAGIX*, Registration no. 70825, <www.dmirs.wa.gov.au/geoview>.
- Chandler, VW and Lively, RS 2014, Evaluation of horizontal-to-vertical spectral ratio (HVSR) passive seismic method for estimating the thickness of Quaternary deposits in Minnesota and adjacent parts of Wisconsin: *Minnesota Geological Survey, Open File Report 14-01*, 52p.
- Collins, C, Kayen, R, Carlin, B, Allen, T, Cummins, P and McPherson, A 2006, Shear-wave velocity measurements at Australian ground motion seismometer sites by the spectral analysis of surface waves (SASW) method, Canberra, 2006/11/24: Australian Earthquake Engineering Society Conference, Proceedings of Earthquake Engineering in Australia, p. 173–178, 6p.
- Feldpausch, SA 2017, Gravity and Passive Seismic Methods Used Jointly for Understanding the Subsurface in a Glaciated Terrain: Dowling and Maple Grove Quadrangles, Barry Country, Michigan, no. 923: Western Michigan University, Michigan, USA, Master of Science thesis (unpublished), 90p.
- Geological Survey of Western Australia 2020, Magnetic anomaly grids (40 m) of Western Australia (2020 – version 1): Geological Survey of Western Australia, digital data layer, <www.dmirs.wa.gov.au/geophysics>.
- Hastings Technology Metals Limited 2017, Yangibana Project: Definitive Feasibility Study Executive Summary: Hastings Technology Metals Limited.
- Ibs-von Seht, M and Wohlenberg, J 1999, Microtremor measurements used to map thickness of soft sediments: *Bulletin of the Seismological Society of America*, v. 89, no. 1, p. 250–259.
- Jakica, S 2018, Using passive seismic to estimate the thickness of the Leonora Breakaways, Western Australia, in *5th Australian Regolith Geoscientists Association Conference, Conference Proceedings: 5th Australian Regolith Geoscientists Association Conference*, Wallaroo, South Australia, 8–11 April 2018, p. 17–20.
- Jefferson, L and McDougall, K 2019, Geology and drillhole information of Yangibana study area; personal communications between GSWA geologists, Groundwater Resource Management consultant and Hastings Technology Metals Limited geologists, January–February 2019, Perth, Western Australia.
- Jiang, Z, Mallants, D, Peeters, L, Gao, L, Soerensen, C and Mariethoz, G 2019, High-resolution paleovalley classification from airborne electromagnetic imaging and deep neural network training using digital elevation model data: *Hydrology and Earth System Science*, v. 23, no. 6, p. 2561–2580, doi:10.5194/hess-23-2561-2019.
- Krapf, C, Costar, A, Keppel, M, Inverarity, K, Love, A, Stoian, L, Gordon, G, Soerensen, C and Munday, T 2019, Backing up the AEM – unravelling a palaeovalley fill for groundwater exploration in the APY Lands, in *AEGC extended abstracts 2019; proceedings of the Australasian Exploration Geoscience Conference*, Perth, Western Australia, 2–5 September 2019, 6p.
- Kumar, M, Hart, J and Prakash, N 2018, Application of passive seismic in determining overburden thickness: North West Zambia, in *AEGC extended abstracts 2018: proceedings of the Australasian Exploration Geoscience Conference*, Sydney, NSW, 18–21 February 2018.
- Lane, JW, White, EA, Steele, GV and Cannia, JC 2008, Estimation of Bedrock Depth Using the Horizontal-to-Vertical (H/V) Ambient-Noise Seismic Method, in *Symposium on the Application of Geophysics to Engineering and Environmental Problems, Proceedings: Symposium on the Application of Geophysics to Engineering and Environmental Problems 2008*, Philadelphia, Pennsylvania, Denver, Colorado, 6–10 April 2008: Society of Exploration Geophysicists.
- Mackey, T, Lawrie, K, Wilkes, P, Munday, T, de Souza Kovacs, N, Chan, R, Gibson, D, Chartres, C and Evans, R 2000, Palaeochannels near West Wyalong, New South Wales: A case study in delineation and modelling using aeromagnetism: *Exploration Geophysics*, v. 31, p. 1–7.
- Martin, DMcB, Thorne, AM and Occhipinti, SA 2004, Edmund, WA Sheet 2150: Geological Survey of Western Australia, 1:100 000 Geological Series.
- Meyers, J 2017, Passive seismic surveying background, methods and HVSR case studies: Australian Institute of Geoscientists Workshop, Brisbane, 02 May 2017: Australian Institute of Geoscientists.
- Micromed 2009, The Short Tromino How To: What should I do now?: MoHo Science and Technology, Treviso, Italy, 26p.
- Micromed 2012, Introduction to the H/V modelling routine for stratigraphic purposes in Grilla: Micromed S.p.A., Mogliano Veneto, Italy, 21p., <http://tromino.eu>.
- MoHo 2017, Tromino Portable ultra-light acquisition system for seismic noise and vibrations: User's Manual: MoHo Science and Technology, Venice, Italy, 148p., <www.moho.world>.
- MoHo Science and Technology 2017, Export Price List 2017: MoHo Science and Technology, Venice, Italy, <www.moho.world>.
- Munday, T, Soerensen, C, Marchant, D, Silic, J, Paterson, R, Viezzoli, A, Kunzmann, M and Spinks, S 2018, 1, 2.5 and/or 3D Inversion of Airborne EM data – options in the search for sediment-hosted base metal mineralisation in the McArthur Basin, Northern Territory, in *ASEG extended abstracts 2018; proceedings of the Australasian Exploration Geoscience Conference*, Sydney, 18–21 February 2018, p. 1–8.
- Nakamura, Y 1989, A method for dynamic characteristics estimation of subsurface using microtremor on the ground: *Quarterly Report of the Railway Technical Research Institute*, v. 30, no. 1, p. 25–33.
- Owers, MC, Meyers, JB, Siggs, B and Shackleton, M 2016, Passive seismic surveying for depth to base of paleochannel mapping at Lake Wells, Western Australia, in *ASEG extended abstracts 2016; proceedings of the 25th International Geophysical Conference and Exhibition*, Adelaide, South Australia, 21–24 August, 9p.
- Paterson, R 2019, Final Report – 2.5D Inverse Modelling of AEM TEMPEST 25 Hz Data: Area 1 (Fortnum), Area 2 (Edmund Station) Capricorn Region, WA: Intrepid Geophysics and Geointrepid Geophysical Software Technology and Consulting Specialists, Melbourne, Australia (unpublished), 26p.
- Paterson, R, Silic, J, Fitzgerald, DJ and Jakica, S 2017, High accuracy 2.5D AEM inversion method for banded iron-formation (BIF) and other geological settings, in *AusIMM extended abstracts; Iron Ore 2017 Conference*, Perth, Western Australia, 24–26 July 2017, 18p.

- Petheram, C, McMahon, TA and Peel, MC 2008, Flow characteristics of rivers in northern Australia: Implications for development: *Journal of Hydrogeology*, v. 357, p. 93–111, doi:10.1016/j.jhydrol.2008.05.008.
- Roach, IC 2018, Application of AEM for cover thickness mapping in the southern Thomson Orogen, *in* AEGC extended abstracts 2018; proceedings of the Australasian Exploration Geoscience Conference, Sydney, NSW, 18-21 February 2018, 6p.
- Scheib, AJ 2014, The application of passive seismic to estimate cover thickness in greenfields areas of Western Australia – method, data interpretation and recommendations: Geological Survey of Western Australia, Record 2014/9, 67p.
- SESAME European Research Project 2004, Guidelines for the implementation of the H/V spectral ratio technique on ambient vibrations – measurements, processing and interpretation: European research project WP12 – Deliverable D23.12: European Commission – Research General Directorate, December 2004, 62p.
- Silic, J, Paterson, R and Fitzgerald, DJ 2018, 2.5D vs 1D AEM Forward and Inversion Methods at a Survey Scale: A Case Study, *in* ASEG extended abstracts: Australasian Exploration Geoscience Conference, Sydney, 8p.
- Silic, J, Paterson, R, Fitzgerald, DJ and Archer, T 2015, Comparing 1D and 2.5D AEM inversions using a new adaptive inversion solver in a 3D geological mapping environment, *in* European Association of Geoscientists and Engineers (EAGE) extended abstracts 2015; proceedings of the first European Airborne Electromagnetics Conference, Turin, Italy, 6-10 September 2015, 5p.
- Smith, NRA, Reading, AM, Asten, MW and Funk, CW 2013, Depth to basement and seismic velocity structure from passive seismic soundings in central Australia: ASEG extended abstracts 2013; proceedings of the 23rd International Geophysical Conference and Exhibition, Melbourne, Victoria, 11–16 August 2013, 4p.
- Wilson, GA, Raiche, AP and Sugeng, F 2006, 2.5D inversion of airborne electromagnetic data: *Exploration Geophysics*, v. 37, no. 4, p. 363–371.
- Winmar, RY and Bracknell, K 2021, Perth Festival 2021, *in* Perth Festival 2021 Program, Perth, Western Australia, 5–28 February 2021, 41p.

This Record is published in digital format (PDF) and is available as a free download from the DMIRS website at <www.dmirs.wa.gov.au/GSWApublications>.

Further details of geoscience products are available from:

Information Centre
Department of Mines, Industry Regulation and Safety
100 Plain Street
EAST PERTH WESTERN AUSTRALIA 6004
Phone: +61 8 9222 3459 Email: publications@dmirs.wa.gov.au
www.dmirs.wa.gov.au/GSWApublications

